

Conformationally Restricted σ_1 Receptor Antagonists from
(-)-Isopulegol

Luca Blicher, Rafael González-Cano, Erik Laurini, Francisco R. Nieto, Judith Schmidt, Dirk Schepmann, Sabrina Pricl, and Bernhard Wünsch*

Cite This: *J. Med. Chem.* 2023, 66, 4999–5020

Read Online

ACCESS |



Metrics & More

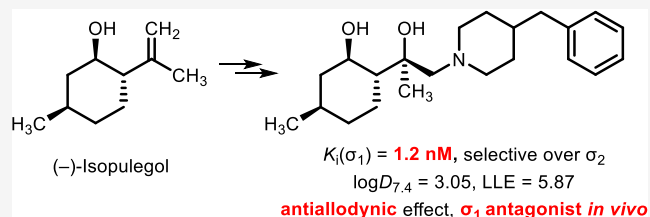


Article Recommendations



Supporting Information

ABSTRACT: Antagonists at σ_1 receptors have great potential for the treatment of neuropathic pain. Starting from monoterpene (-)-isopulegol (**1**), aminodiols **8–11** were obtained and transformed into bicyclic **13–16** and tricyclic ligands **19–22**. Aminodiols **8–11** showed higher σ_1 affinity than the corresponding bicyclic **13–16** and tricyclic derivatives **19–22**. (*R*)-configuration in the side chain of aminodiols (**8** and **10**) led to higher σ_1 affinity than (*S*)-configuration (**9** and **11**). 4-Benzylpiperidines (**b**-series) revealed higher σ_1 affinity than 4-phenylbutylamines (**a**-series). Aminodiol **8b** showed very high σ_1 affinity ($K_i = 1.2$ nM), excellent selectivity over σ_2 receptors, and promising $\log D_{7.4}$ (3.05) and lipophilic ligand efficiency (5.87) values. Molecular dynamics simulations were conducted to analyze the σ_1 affinity and selectivity on an atomistic level. In the capsaicin assay, **8b** exhibited similar antiallodynic activity to the prototypical σ_1 antagonist S1RA. The antiallodynic activity of **8b** was removed by co-application of the σ_1 agonist PRE-084, proving σ_1 antagonism being involved in the antiallodynic effect.



1. INTRODUCTION

σ Receptors comprise σ_1 and σ_2 receptor subtypes, which are related pharmacologically but not evolutionarily. σ_1 Receptors are located primarily in the endoplasmic reticulum of cells in the central nervous system (CNS) and the periphery. The biological functions of σ_1 receptors in healthy tissues and cancer are not thoroughly understood,^{1,2} and currently, an endogenous ligand is not known. However, σ_1 receptors participate in pathological processes such as depression, chronic pain, schizophrenia, alcoholism, and neurodegenerative disorders.³ σ_1 Receptors are overexpressed in tumor cells. Therefore, σ_1 receptor ligands are potential anticancer drugs, either as apoptosis-inducing agents or as drug carriers.^{4,5} Moreover, appropriately labeled σ_1 ligands are tracers in positron emission tomography (PET) for the diagnosis of cancer⁶ or CNS disorders.^{7,8}

The first X-ray crystal structure of the σ_1 receptor was published in 2016. It reveals that σ_1 receptor proteins form homotrimers, with a single transmembrane domain for each protomer.⁹ Co-crystallized ligands are located in a β -barrel motif of the cytosolic carboxy-terminal domain. The protonated amino group of the ligands forms an ionic interaction with Glu172, which is supported by Tyr103 and Asp126, in an otherwise hydrophobic binding pocket.⁹ X-ray crystal structure analysis and molecular dynamics (MD) simulations suggest that agonists occupy a different portion of the same pocket than antagonists, which changes the conformation of the helix $\alpha 4$ of the receptor.¹⁰

These interactions are in line with earlier empiric pharmacophore models, which postulates that potent σ_1 ligands need a basic amino moiety that connects two or more lipophilic groups with distances of 2.5–3.9 and 6–10 Å, respectively.¹¹

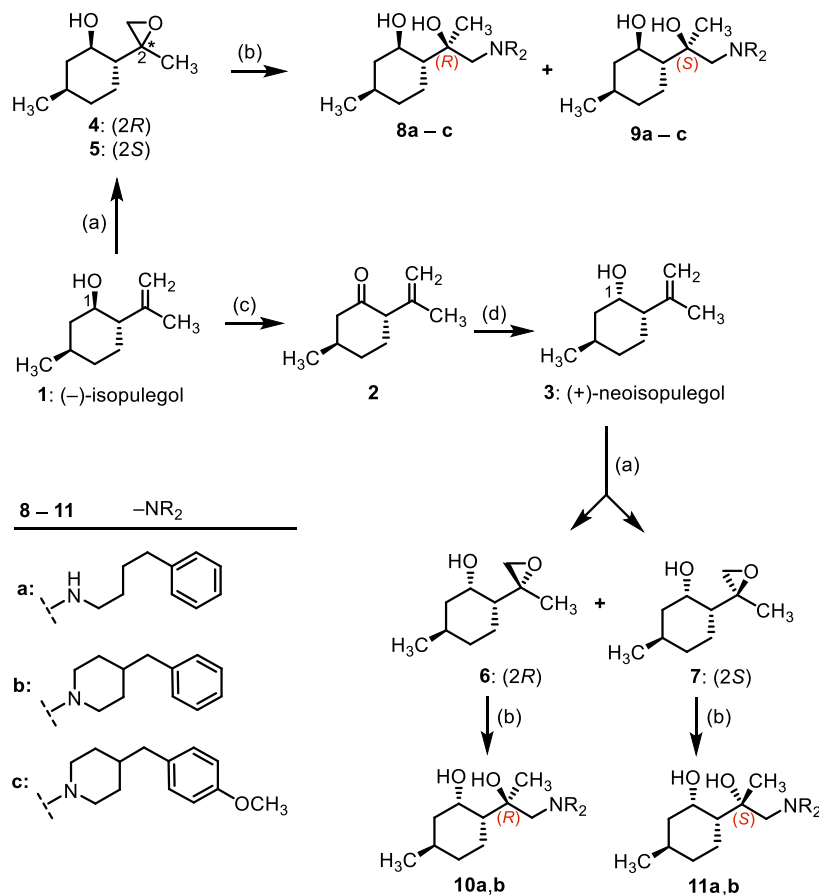
σ_1 Receptor antagonists emerge as interesting drug candidates for the treatment of different types of pain. σ_1 Receptor ligands modulate opioid receptor-mediated activity.^{12–14} Although σ_1 receptor antagonists themselves are not able to reduce acute pain, they increase the analgesic activity of opioid receptor agonists, without increasing side effects.¹⁵ Neuropathic pain is caused by a lesion or a disease of the peripheral or central somatosensory nervous system¹⁶ and resists treatment by non-steroidal anti-inflammatory drugs and opioid analgesics.² However, σ_1 receptor knockout mice show reduced pain reactions in chemical^{17,18} and neuropathic pain models.^{19,20} Antagonism of σ_1 receptors reduces amplification of pain signals within the CNS.² The σ_1 receptor antagonist E-52862 (S1RA)²¹ is currently in clinical trials for the treatment of neuropathic pain.^{22,23}

According to pharmacophore models,¹¹ a basic amino group and two lipophilic substituents are required to achieve high σ_1

Received: December 20, 2022

Published: March 22, 2023



Scheme 1. Synthesis of Enantiomerically Pure Aminodiols 8–11 from (–)-Isopulegol (1)^a

^aReagents and reaction conditions: (a) *m*CPBA, CH₂Cl₂, rt, 1.8–2.2 h, and 82–90%. (b) Ph(CH₂)₄NH₂ or 4-benzylpiperidine or 4-(4-methoxybenzyl)piperidine, CH₃OH, reflux, 19–40 h, and 47–92%. (c) Dess–Martin periodinane (DMP), CH₂Cl₂, rt, and 93%. (d) L-Selectride, THF, –78 °C, 4 h, then H₂O₂, NaOH, rt, 20 min, and 67%.

receptor affinity. Sterically demanding substituents are allowed. Usually, potent σ_1 antagonists contain flat aromatic substituents connected via different linkers with the central basic amino moiety. In this project, one aromatic substituent should be replaced by a sp^3 -hybridized scaffold. Since sp^3 -hybridized scaffolds automatically bring stereocenters, several stereoisomers are possible. In order to come up with stereochemically defined pure stereoisomers, we planned a chiral pool synthesis starting with sp^3 -hybridized enantiomerically pure natural products with defined configuration. For this purpose, the cheap, commercially available monoterpenoid (–)-isopulegol (1) was selected as a sp^3 -rich starting material, which should match one lipophilic substituent at the basic amino moiety.

2. RESULTS AND DISCUSSION

2.1. Synthesis of 4-Amino-1,3-diols from (–)-Isopulegol (1).

In the first step, (–)-isopulegol (1) was oxidized with *m*CPBA to afford a mixture of two epimeric epoxides 4 and 5 in a ratio of 60:40.^{52,53} Nucleophilic ring opening of the epoxide with either 4-phenylbutan-1-amine (**a**-series), 4-benzylpiperidine (**b**-series), or 4-(4-methoxybenzyl)piperidine (**c**-series) yielded aminodiols 8a–c and 9a–c, which were separated by flash chromatography (fc), respectively (Scheme 1).

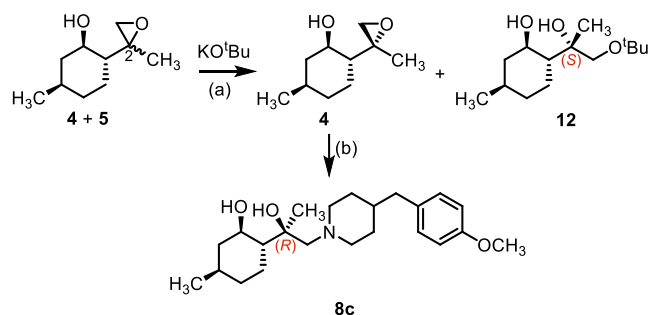
To invert the configuration of the center of chirality in 1-position, (–)-isopulegol (1) was oxidized with DMP to obtain isopulegone (2), which was reduced by the sterically demanding reducing agent L-selectride to afford diastereoselectively (+)-neoisopulegol (3) in 62% overall yield.²⁴ *m*CPBA oxidized 3 to obtain the diastereomeric epoxides 6 and 7, which were separated by fc. Both epoxides 6 and 7 reacted with the primary amine 4-phenylbutan-1-amine (**a**-series) and the secondary amine 4-benzylpiperidine (**b**-series) to provide the aminodiols 10a,b and 11a,b.

Aminodiols 8 with (*R*)-configuration in the side chain exhibited higher σ_1 receptor affinity than epimers 9 with (*S*)-configuration. Hence, diastereoselective access to (*R*)-epoxide 4 was of interest. Reaction of a mixture of 4 and 5 with KO^tBu in *tert*-BuOH selectively transformed (*S*)-configured epoxide 5 into *tert*-butyl ether 12, while (*R*)-configured epoxide 4 did not react (Scheme 2). Subsequently, the crude product mixture was treated with 4-(4-methoxybenzyl)piperidine to convert the remaining epoxide 4 into β -aminoalcohol 8c. With this method, the more potent β -aminoalcohols 8 could be obtained without time-consuming separation of diastereomers (compare Scheme 1).

2.2. Rigidization of the Scaffold and Elucidation of the Absolute Configuration.

The configuration of the newly generated center of chirality of the tertiary alcohol in aminodiols 8–11 could not be determined unequivocally by nuclear magnetic resonance (NMR) spectroscopy. To assign

Scheme 2. Reaction of Epoxide Mixture 4 + 5 with KO^tBu and Subsequently with 4-(4-Methoxybenzyl)piperidine^a



^aReagents and reaction conditions: (a) KO^tBu, *tert*-BuOH, 60 °C, and 16 h. (b) 4-(4-Methoxybenzyl)piperidine, CH₃OH, reflux, 45 h, and 33% (two steps).

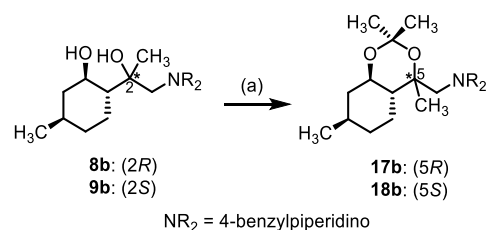
the relative and thus absolute configuration, aminodiols 8a,b–11a,b were converted into conformationally restricted acetals 13a,b–16a,b (Scheme 3). For this purpose, the aminodiols 8a,b–11a,b were reacted with dimethoxymethane and *p*-toluenesulfonic acid in a transacetalization reaction to yield the acetals 13a,b–16a,b.

In a 2D NOESY experiment on 13a, the proton in 1-position and the CH₃ moiety in 5-position correlated because both are axially oriented (Scheme 3, bottom). In 14a, the aminomethyl moiety is axially oriented instead of the CH₃ moiety, giving a cross peak between 1-H and 5-CH₂NR₂. Hence, (5*R*)- and (5*SS*)-configurations were assigned to 13a and 14a, respectively. For 15a and 16a, the orientation of the proton in 1-position relative to the substituent in 5-position was analyzed by the same strategy, which allowed the unequivocal assignment of (5*R*)- and (5*SS*)-configuration, respectively. The relative and

finally absolute configuration of the chiral center in the side chain of the aminodiols 8–11 was derived from the configuration of the rigid acetals 13–16. The results obtained by the 2D NOESY experiments for the a-series discussed above were transferred to the b-series and further analogues.

To increase diversity, 2,2-dimethoxypropane (acetone dimethyl ketal) was reacted with epimeric diols 8b and 9b to afford annulated dioxanes 17b and 18b, respectively (Scheme 4). Compared to 13b and 14b, they contain two

Scheme 4. Conversion of Aminodiols 8b and 9b into Ketals 17b and 18b^a

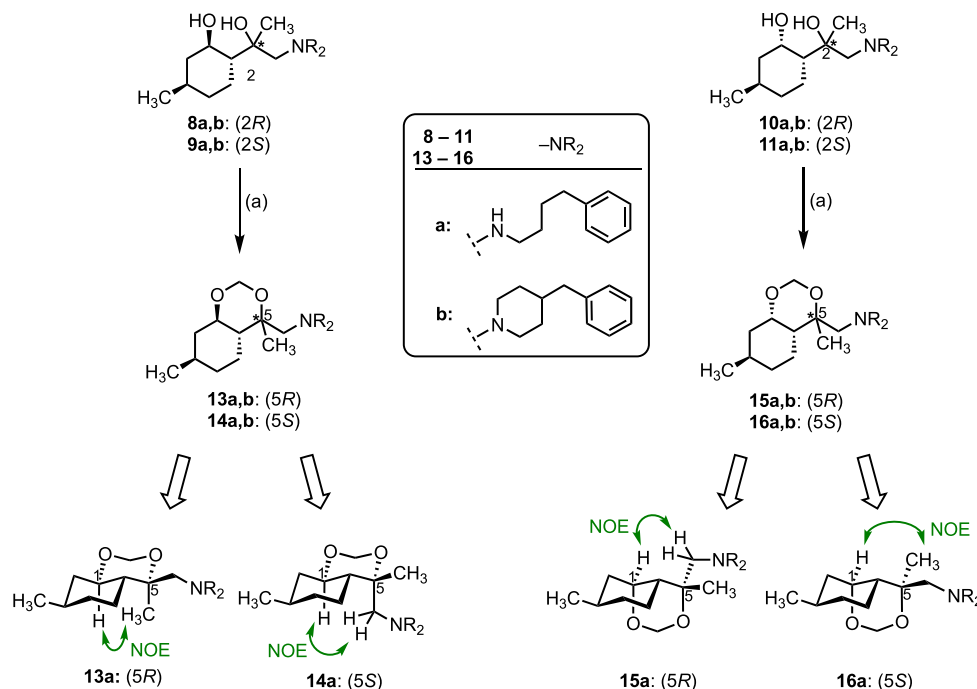


^aReagents and reaction conditions: (a) 2,2-dimethoxypropane, *p*TsOH, DMF, 70 °C, 5 h, and 27–48%

additional CH₃ groups at the ketalic center. 2D NOESY experiments recorded for 17b and 18b allowed the unequivocal assignment of the absolute configuration of the newly generated center of chirality in 5-position, which confirms the absolute configuration of the corresponding precursors 8b and 9b.

2.3. Synthesis of Tricyclic Dioxazatricyclo[7.3.1.0^{3,8}]-tridecanes 19–22. To further increase the selectivity for the σ₁ receptor, the scaffold was further rigidified to exploit the plasticity of the σ₁ receptor binding site. To meet this criterion,

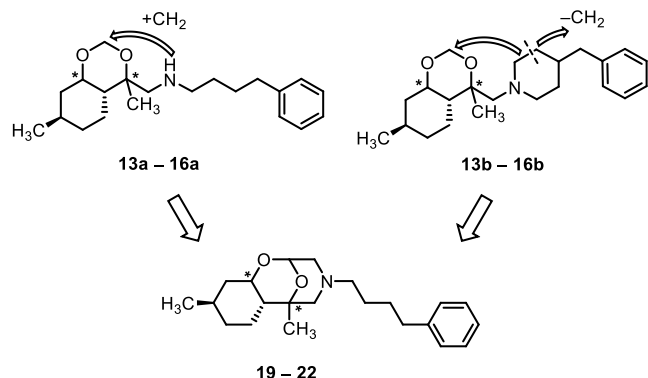
Scheme 3. Conversion of Aminodiols 8a,b–11a,b into Acetals 13a,b–16a,b and Determination of the Relative and Absolute Configuration by NOESY Experiments^a



^aReagents and reaction conditions: (a) dimethoxymethane, *p*TsOH, rt–40 °C, 4–72 h, and 33–92%.

tricyclic compounds **19–22** were designed that contain an additional CH₂ moiety connecting the amino moiety with the acetalic methylene moiety of the phenylbutylamines **13a–16a** (a-series) (Scheme 5). Similarly, rigidization of benzylpiper-

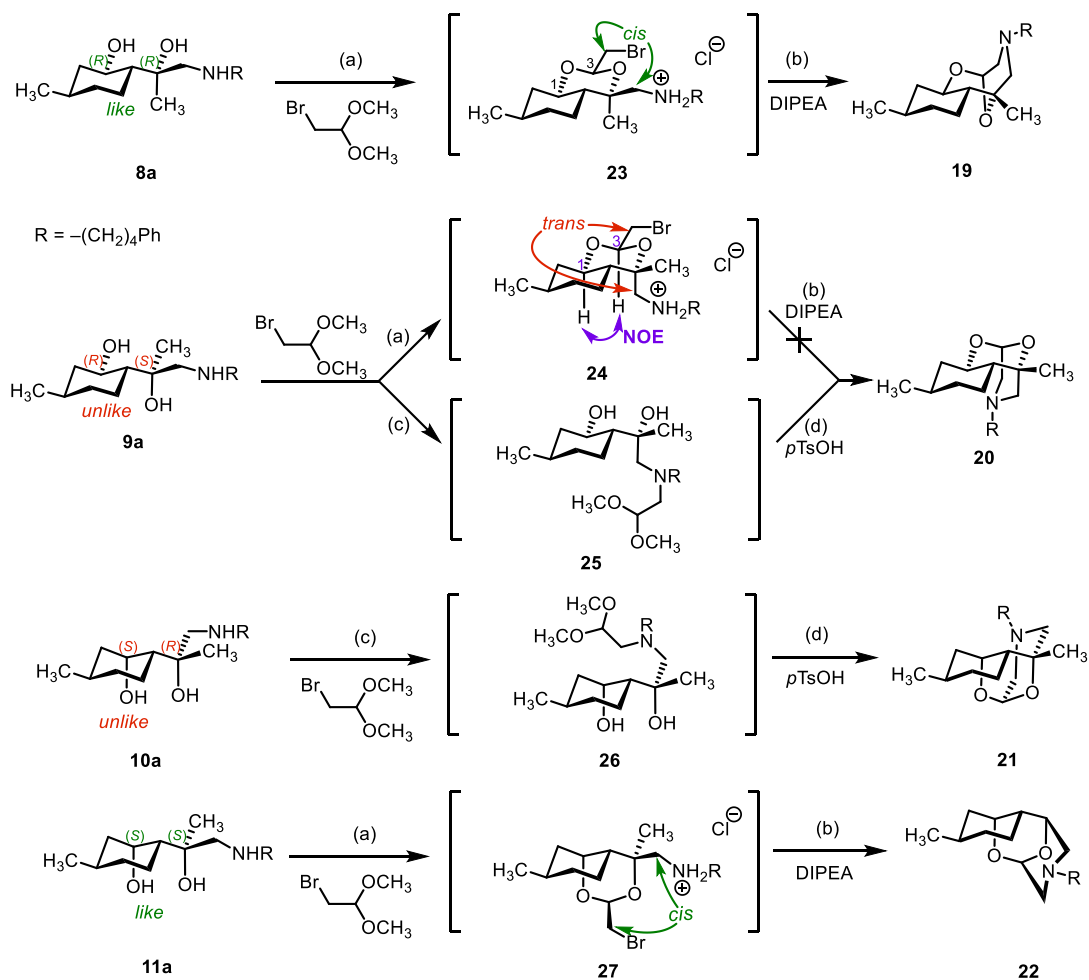
Scheme 5. Design of Tricyclic σ Receptor Ligands **19–22 as Rigid Analogues of Acetals **13a,b–16a,b****



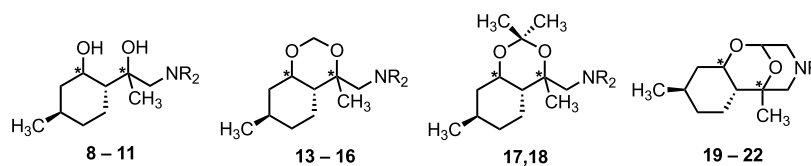
idine derivatives **13b–16b** (b-series) leads to the same scaffold: a CH₂ moiety of the piperidine ring is removed, and the remaining CH₂ moiety is connected to the acetalic CH₂ moiety.

The methylene bridge was introduced into aminodiols **8a** by transacetalization with 2-bromoacetaldehyde dimethyl acetal under acidic conditions (Scheme 6). After complete conversion, the bicyclic intermediate **23** was deprotonated with DIPEA, which led to the tricyclic product **19** by an intramolecular S_N2 reaction. The relative configuration of the C-atoms bearing the OH groups in the starting materials determined the outcome of this one-pot procedure. **8a** with (*R*)-configuration at both centers of chirality (like configuration) provided the tricyclic product **19** in 58% yield, whereas the corresponding unlike configured diastereomer **9a** with (*R,S*)-configuration did not form a tricyclic product. In the intermediate **23**, the bromomethyl moiety adopts the thermodynamically favored equatorial orientation, i.e., in **23**, the bromomethyl and aminomethyl groups are *cis*-oriented, allowing the subsequent intramolecular S_N2 reaction to give **19**. However, in intermediate **24** originating from **9a**, the bromomethyl moiety in 2-position and the aminomethyl

Scheme 6. Synthesis of Tricyclic σ_1 Receptor Ligands **19–22 by Condensation of Diastereomeric Aminodiols **8a–11a** with 2-Bromoacetaldehyde Acetal^a**



^aReagents and reaction conditions: (a) 2-bromoacetaldehyde dimethyl acetal, *p*TsOH, CHCl₃, 50 °C, and 16 h. (b) DIPEA, 60 °C, and 96 h. **19**: 58%, **22**: 55%. (c) 2-Bromoacetaldehyde dimethyl acetal, K₂CO₃, DMF, 130 °C, and 20–22 h. (d) *p*TsOH, 80 °C, and 1.5–3.5 h. **20**: 19%; **21**: 33%.

Table 1. σ_1 , σ_2 , and GluN2B Affinity of Enantiomerically Pure 1,3-Diols 8–11 and Their Bicyclic and Tricyclic Analogues 13–22^b

| compd. | NR ₂ /NR | $K_i \pm \text{SEM} [\text{nM}]^a$ | | | σ_1 receptor selectivity | |
|------------------------------|--------------------------------------|------------------------------------|------------|-----------|---------------------------------|--------------------------|
| | | σ_1 | σ_2 | GluN2B | σ_1/σ_2 | $\sigma_1/\text{GluN2B}$ |
| 8a | NH(CH ₂) ₄ Ph | 8.2 ± 1.2 | 850 | 1300 | 104 | 159 |
| 9a | NH(CH ₂) ₄ Ph | 31 ± 2 | 207 | 508 | 6 | 16 |
| 10a | NH(CH ₂) ₄ Ph | 7.0 ± 2.1 | 424 ± 125 | 1060 | 61 | 151 |
| 11a | NH(CH ₂) ₄ Ph | 43 ± 13 | 265 | 511 ± 36 | 6 | 12 |
| 8b | 4-Bn-Pip | 1.2 ± 0.16 | 36 ± 6 | 53 ± 8 | 30 | 44 |
| 9b | 4-Bn-Pip | 2.8 ± 0.7 | 194 ± 26 | 92 ± 19 | 69 | 33 |
| 10b | 4-Bn-Pip | 1.0 ± 0.09 | 172 ± 31 | 125 ± 27 | 167 | 121 |
| 11b | 4-Bn-Pip | 18 ± 2 | 216 ± 46 | 363 ± 82 | 12 | 20 |
| 8c | 4-MeO-Bn-Pip | 2.9 ± 0.2 | 75 ± 8 | 45 ± 7 | 26 | 16 |
| 8c + 9c | 4-MeO-Bn-Pip | 4.4 ± 1.1 | 87 ± 9 | 131 ± 21 | 20 | 30 |
| 13a | NH(CH ₂) ₄ Ph | 69 ± 17 | 86 ± 6 | 61 ± 14 | 1.2 | 0.88 |
| 14a | NH(CH ₂) ₄ Ph | 9.7 ± 3.0 | 322 ± 108 | 408 ± 104 | 33 | 42 |
| 15a | NH(CH ₂) ₄ Ph | 8.6 ± 0.8 | 525 | 313 | 61 | 36 |
| 16a | NH(CH ₂) ₄ Ph | 42 ± 7 | 273 | 263 | 6.5 | 6.3 |
| 13b | 4-Bn-Pip | 5.0 ± 0.9 | 119 ± 9 | 36 ± 13 | 24 | 7.2 |
| 14b | 4-Bn-Pip | 1.6 ± 0.3 | 379 | 370 ± 67 | 237 | 234 |
| 15b | 4-Bn-Pip | 4.9 ± 0.9 | 145 ± 22 | 205 ± 51 | 30 | 42 |
| 16b | 4-Bn-Pip | 3.5 ± 0.7 | 123 ± 19 | 267 | 35 | 76 |
| 17b | 4-Bn-Pip | 16 ± 2 | 649 | 1300 | 41 | 81 |
| 18b | 4-Bn-Pip | 114 ± 33 | 880 | 423 | 7.7 | 3.7 |
| 19 | N(CH ₂) ₄ Ph | 2100 | 0% | 6% | | |
| 20 | N(CH ₂) ₄ Ph | 805 | 1600 | 0% | | |
| 21 | N(CH ₂) ₄ Ph | 725 | 0% | 0% | | |
| 22 | N(CH ₂) ₄ Ph | 54 ± 8 | 779 | 890 | 14 | 16 |
| (+)-pentazocine | 5.4 ± 0.5 | nd | nd | | | |
| haloperidol | 6.2 ± 1.6 | 78 ± 2.3 | nd | 13 | | |
| di- <i>o</i> -tolylguanidine | 89 ± 29 | 57 ± 18 | nd | 0.6 | | |
| (<i>R,R</i>)-ifenprodil | 125 ± 24 | 98 ± 34 | 5.8 ± 1.3 | 0.8 | 0.05 | |
| E-52862 (S1RA) ²¹ | 17.0 ± 7.0 | >1000 | | >58 | | |
| BD-1063 ²⁹ | 9.15 ± 1.28 | 449 ± 11 | | 49 | | |

^a K_i values ± SEM are means of three independent experiments ($n = 3$). K_i values without SEM represent the mean of two experiments. Values in % represent the inhibition of the radioligand binding at a test compound concentration of 1 μM . ^bThe K_i values of the prototypical σ_1 ligands E-52862²¹ and BD-1063²⁹ were recorded in a different lab.

moiety in 4-position are trans-oriented and thus cannot react with each other. The relative configuration of **24** was confirmed by the 2D NOESY correlation between 1-H and 3-H (Scheme 6).

However, this problem was solved by reversing the reaction steps. First, **9a** was alkylated with 2-bromoacetaldehyde dimethyl acetal in a S_N2 reaction under basic conditions at 130 °C to form the intermediate aminoacetaldehyde dimethyl acetal **25**. Subsequent acid-catalyzed intramolecular transacetalization of **25** furnished the tricyclic product **20**.

For the synthesis of **21** and **22** from (+)-neoisopulegol derivatives **10a** (unlike-configuration) and **11a** (like-configuration), the same synthetic strategies were followed. The reaction of like-configured aminodiols **11a** with bromoacetaldehyde dimethyl acetal under acidic conditions provided predominantly 1,3-dioxane **27**. *cis*-Orientation of the bromomethyl and aminomethyl moieties ensured the cyclization after deprotonation of **27** with DIPEA to give **22**. Its diastereomer

21 was obtained by alkylation of secondary amine **10a** with bromoacetaldehyde dimethyl acetal and subsequent intramolecular transacetalization.

2.4. Receptor Affinity In Vitro. The affinity to σ_1 and σ_2 receptors, as well as NMDA receptors with the GluN2B subunit, was recorded in competitive receptor binding assays using [³H]-labeled radioligands. The σ_1 receptor binding assay was performed by incubation of membrane preparations from guinea pig brain with the test compound in the presence of the radioligand [³H]-(+)-pentazocine. In the σ_2 receptor binding assay, the non-subtype-selective σ receptor ligand [³H]di-*o*-tolylguanidine was used in the presence of an excess of non-labeled (+)-pentazocine.^{25–27} The affinity to the ifenprodil binding site of NMDA receptors containing the GluN2B subunit was determined with [³H]-labeled ifenprodil and cell membrane preparation from stably transfected mouse fibroblast L(tk-) cells.²⁸ Table 1 summarizes the affinity data of the prepared ligands.

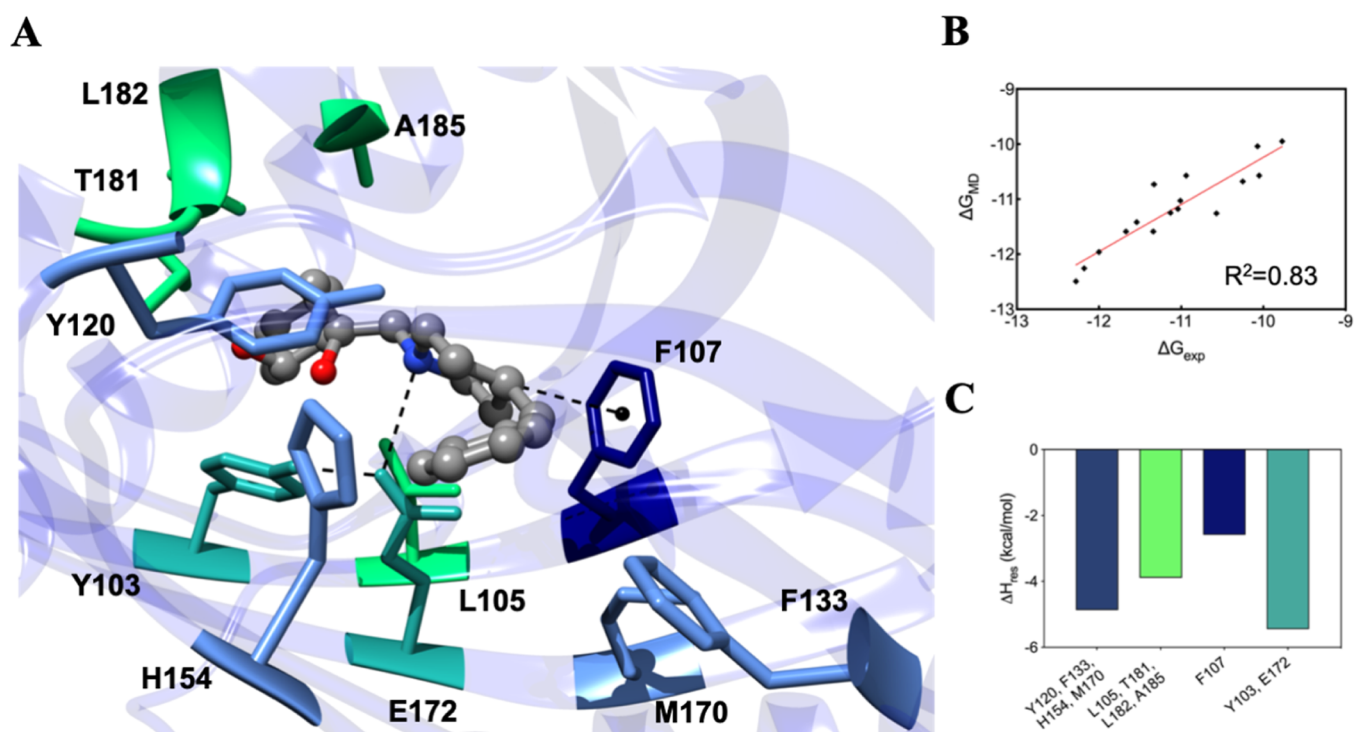


Figure 1. (A) Atomistic details of compound **10b** in the binding pocket of the σ_1 receptor. The side chains of the main interacting σ_1 residues are represented as colored sticks and labeled. The ligand is shown as atom-colored sticks and balls (C, gray; N, blue; and O, red). Hydrogen atoms, water molecules, ions, and counterions are omitted for clarity. (B) Free energy values (ΔG_{MD}) obtained from MD simulations and their correlation with the corresponding experimental values (ΔG_{EXP}) extrapolated from the experimentally determined K_i values (see Table 1) using the relationship $\Delta G_{\text{EXP}} = -RT \ln(1/K_i)$. (C) Per-residue binding free energy decomposition of the main interacting residues of the $\sigma_1/10b$ complex.

The synthesized enantiomerically pure 1,3-diols **8–11** and their bicyclic analogues **13–16** display very high σ_1 receptor affinity with K_i values between 1.0 and 69 nM. Compared to formaldehyde acetals **13b** and **14b**, acetonides **17b** and **18b** and the tricyclic analogues **19–22** bearing the 4-phenylbutyl moiety exhibit considerably lower σ_1 affinity. For the aminodiols **8–11**, a correlation between the stereochemistry and σ_1 affinity was detected: stereoisomers **8** and **10** with (*R*)-configuration in the aminohydroxypropan-2-yl side chain show higher σ_1 affinity than their (*S*)-configured diastereomers **9** and **11**. In both the aminodiol series **8–11** and the bicyclic ligand series **13–16**, 4-benzylpiperidino derivatives (**b**-series) reveal higher σ_1 affinity than the 4-phenylbutyl-substituted secondary amines (**a**-series), respectively.

The conversion of aminodiols **8–11** into bicyclic ligands **13–16** removed two H-bond donors and reduced the conformational flexibility. As a trend, some of the flexible and more polar aminodiols reveal higher σ_1 affinity than their more rigid and less polar bicyclic counterparts, e.g., $K_i(\mathbf{8a}) = 8.2$ nM; $K_i(\mathbf{13a}) = 69$ nM and $K_i(\mathbf{8b}) = 1.2$ nM; and $K_i(\mathbf{13b}) = 5.0$ nM.

The particularly high σ_1 affinity of the aminodiols **8b–10b** and the bicyclic analogues **13b–16b** with K_i values below 5 nM has to be emphasized.

2.5. Receptor Selectivity. The affinity toward σ_2 receptors was also recorded in receptor binding studies. Since the pharmacophore of σ ligands is similar to the pharmacophore of ligands interacting with the ifenprodil binding site of GluN2B receptors and we often observe cross-reactivity,^{30–32} the interaction with GluN2B subunit-containing NMDA receptors was included in this study. The aminodiols **8–11** and their bicyclic analogues **13–16** exhibit high selectivity for σ_1

receptors over σ_2 receptors and the ifenprodil binding site of GluN2B-NMDA receptors. Due to the low receptor affinities of the tricyclic ligands **19–21**, selectivity factors could only be determined for **22**, displaying moderate selectivity for σ_1 receptors. Particularly high selectivity was observed for ligands with very high σ_1 affinity. With respect to σ_1 affinity and selectivity, the aminodiols **8a**, **10a**, and **8b–10b** as well as the bicyclic analogues **13b–16b** represent the most promising σ_1 ligands of this study.

The bicyclic 4-phenylbutylamine **13a** is a multiple receptor ligand since it binds to σ_1 , σ_2 , and GluN2B-NMDA receptors with similar affinity.

2.6. Computational Studies on Receptor Affinity. In order to acquire more details about how these new molecules bind to their biological target, the complexes between σ_1 receptor and compounds **8a–11a**, **8b–11b**, **13a–16a**, and **13b–16b** were subjected to 50 ns of MD simulations. These calculations were performed starting from the 3D structure of the σ_1 receptor protein as determined by X-ray crystal structure analysis (pdb code SHK1).³³ Consequently, using a consolidated computational technique,^{34–36} an ideal binding site for all σ_1 receptor/ligand complexes was initially found in the classic σ_1 binding cavity (Figure 1A). The corresponding ligand/protein free energy of binding (ΔG_{MD}) values and its enthalpic and entropic components (ΔH_{MD} and $-T\Delta S_{\text{MD}}$, respectively) were subsequently obtained through the MM/PBSA (molecular mechanics/Poisson–Boltzmann surface area) approach³⁷ on the resulting σ_1 receptor/ligand complex MD trajectories (Figure 1B and Table S1). As shown in Figure 1B, the calculated binding energy values are in good agreement with those obtained from the experimental σ_1 affinity assay as testified by the high correlation coefficient. Finally, the per-

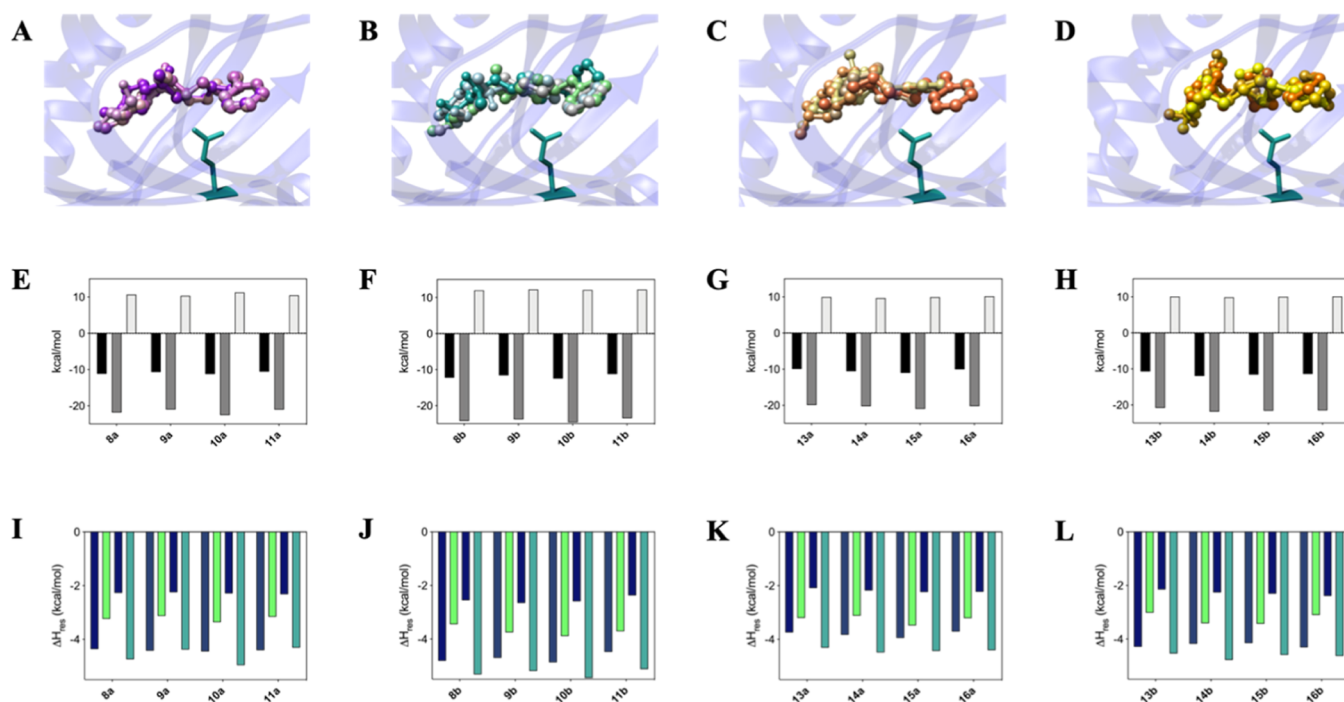


Figure 2. (A–D) Overlay of σ_1 binding modes of compounds **8a–11a** (A, **8a** orchid, **9a** pink, **10a** plum, and **11a** purple), **8b–11b** (B, **8b** light gray, **9a** light green, **10a** light blue, and **11a** light sea green), **13a–16a** (C, **13a** Khaki, **14a** sandy brown, **15a** coral, and **16a** tan), and **13b–16b** (D, **13b** gold, **14b** goldenrod, **15b** yellow, and **16b** orange). (E–H) Comparison between σ_1 receptor calculated free energy of binding (ΔG_{MD} , black), enthalpic (ΔH_{MD} , dark gray), and entropic ($-T\Delta S_{MD}$, light gray) components of compounds **8a–11a** (E), **8b–11b** (F), **13a–16a** (G), and **13b–16b** (H). (I–L) Comparison between σ_1 receptor PRBFED analysis of compounds **8a–11a** (I), **8b–11b** (J), **13a–16a** (K), and **13b–16b** (L). For the color code of each contribution, please refer to Figure 1C.

residue binding free energy deconvolution (PRBFED) of the enthalpic terms (ΔH_{RES}) was used to clarify the precise binding process and the particular ligand/protein interactions.

Interestingly, all compounds share a similar interaction pattern in the σ_1 binding cavity. Specifically, taking as the proof-of-principle compound **10b** as the best σ_1 ligand of the series (Figure 1A), the benzyl moiety and the hydrocarbon spacer can be properly housed in a σ_1 hydrophobic region by engaging favorable van der Waals and aromatic interactions with the side chain of residues Y120, F133, H154, and M170 ($\Sigma\Delta H_{RES} = -4.87$ kcal/mol, Figure 1C and Table S2). The cyclohexanol moiety is nested in another lipophilic cavity underlying σ_1 residues L105, T181, L182, and A185 ($\Sigma\Delta H_{RES} = -4.87$ kcal/mol). It is important to note at this point the two hydroxy groups of the molecule appear to be unessential for binding to the σ_1 receptor. In fact, in the relevant MD simulation, just a weak and not crucial polar interaction with the alcoholic side chain of T181 appears to be the only specific interaction of the OH groups. Undoubtedly, the charged nitrogen atom present in all of the new compounds performs the most topical σ_1 interaction. This protonated amino group is involved in a virtuous π -cation interaction with the aromatic side chain of F107 ($\Delta H_{RES} = -2.59$ kcal/mol). Furthermore, the same basic *N*-atom strongly stabilizes the binding through a stable salt bridge with the carboxy group of E172, which is oriented in an ideal position by a H-bond with Y103 ($\Sigma\Delta H_{RES} = -5.45$ kcal/mol, Figure 1C and Table S2).

By comparing the binding mode of the new derivatives toward the σ_1 receptor, our computational analysis confirmed the moderate influence of the absolute configuration on the interactions with the target for the cyclohexanol derivatives. Indeed, the (*R*)-configuration of molecules **8** and **10** allows an

optimization of the main interactions with the protein compared to the (*S*)-configuration of derivatives **9** and **11**. In fact, all the interactions with the most involved σ_1 residues are more favorable than the corresponding diastereomers (Figure 2 and Tables S1 and S2). For the bicyclic derivatives **13–16**, on the other hand, the (*R*)-configuration is slightly more penalized in binding the σ_1 receptor: even in this case, the lower affinity is not given by the loss of a specific interaction rather by a non-optimal position in the binding cavity with a consequent and significant decrease of all stabilizing forces (Figure 2 and Tables S1 and S2).

To highlight the most significant differences of the new compounds at the level of molecular determinants, the averaged values (AVG) of the MMPBSA and PRBFED analyses obtained from each stereoisomer in each molecular class can provide a clearer panorama (Figure S1). The cyclohexanol derivatives **8a–11a** ($AVG\Delta G_{MD8a-11a} = -10.92$ kcal/mol) and **8b–11b** ($AVG\Delta G_{MD8b-11b} = -11.90$ kcal/mol) globally demonstrated a greater affinity toward the σ_1 receptor with average ΔG_{MD} values of about 0.5 kcal/mol more favorable than the corresponding bicyclic derivatives **13a–16a** ($AVG\Delta G_{MD13a-16a} = -10.40$ kcal/mol) and **13b–16b** ($AVG\Delta G_{MD13b-16b} = -11.42$ kcal/mol). The most relevant difference consists in the enthalpy contribution and therefore in the optimization and in the improvement of all of the main interactions in the σ_1 binding cavity ($AVG\Delta H_{MD8a-11a} = -21.61$ kcal/mol, $AVG\Delta H_{MD8b-11b} = -24.05$ kcal/mol, $AVG\Delta H_{MD13a-16a} = -20.34$ kcal/mol, and $AVG\Delta H_{MD13b-16b} = -21.45$ kcal/mol, Figure S1A). Essentially, the greater conformational freedom of the cyclohexanol scaffold allows a better adaptation in the σ_1 binding pocket, and the lower entropic penalty ($AVG-T\Delta S_{MD8a-11a} = 10.69$ kcal/mol, $AVG-$

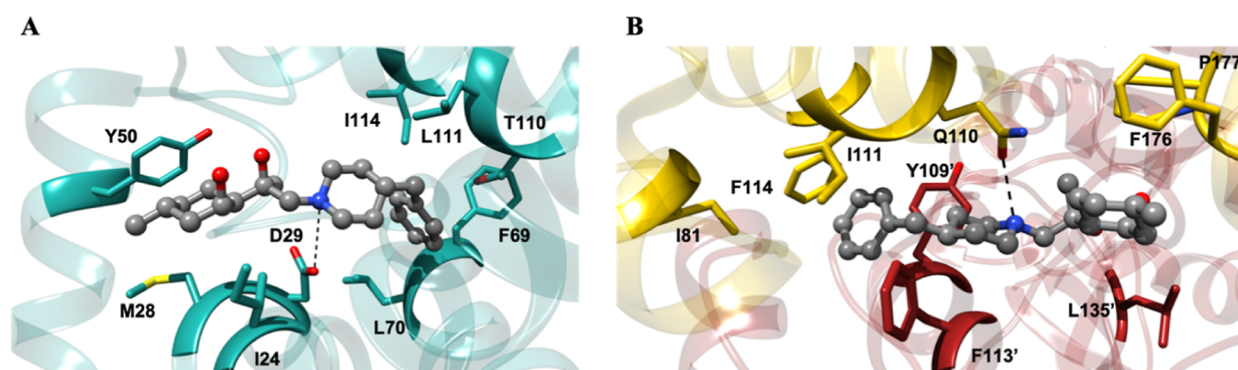


Figure 3. Atomistic details of compound **10b** in complex with σ_2 (A) and NMDA (B) receptors. The side chains of main interacting σ_2 residues are represented as colored sticks and labeled. The subunits of the NMDA receptor dimer are depicted in gold (GluN2B) and in firebrick (GluN1) color. The ligand is shown as atom-colored sticks and balls (C, gray; N, blue; and O, red). Hydrogen atoms, water molecules, ions, and counterions are omitted for clarity.

Table 2. Experimentally Determined $\log D_{7.4}$ Values, σ_1 Affinity, Lipophilic Ligand Efficiency, and Plasma Protein Binding of Selected σ_1 Ligands

| No | Compound | $\log D_{7.4} \pm \text{SEM}$ | $K_i(\sigma_1)$ [nM] | LLE ^{a)} | PPB ^{b)} |
|------------|----------|-------------------------------|----------------------|-------------------|--------------------|
| 8a | | 1.84 ± 0.04 | 8.2 | 6.25 | $92.7 \pm 0.50 \%$ |
| 13a | | 2.67 ± 0.16 | 69 | 4.49 | $93.9 \pm 0.40 \%$ |
| 8b | | 3.05 ± 0.03 | 1.2 | 5.87 | $87.8 \pm 0.51 \%$ |
| 13b | | 3.45 ± 0.08 | 5.0 | 4.85 | $92.2 \pm 0.43 \%$ |
| 19 | | 3.96 ± 0.17 | 2100 | 1.72 | >98 % |

^aLipophilic ligand efficiency (LLE) is defined as $\text{LLE} = \text{p}K_i - \text{clog}P$ (or $\log D$).⁴¹ The experimentally determined $\log D_{7.4}$ value is used in this work.
^bPPB = plasma protein binding.

$T\Delta S_{\text{MD}8\text{b}-11\text{b}} = 12.15$ kcal/mol, $\text{AVG-}T\Delta S_{\text{MD}13\text{a}-16\text{a}} = 9.94$ kcal/mol, and $\text{AVG-}T\Delta S_{\text{MD}13\text{b}-16\text{b}} = 10.02$ kcal/mol, **Figure S1A**) exhibited by the more constrained bicyclic derivatives **13–16** cannot compensate the lower strength of their stabilizing energies.

Finally, the chemical nature of the spacer between the basic N-atom and the phenyl ring plays an essential role in optimizing the binding against σ_1 receptor. Indeed, the new compounds provided with the piperidine spacer, **8b–11b** and **13b–16b**, exhibited a gain of about 1 kcal/mol on the ΔG_{MD} values compared to their corresponding derivatives with the butyl spacer, **8a–11a** and **13a–16a** (**Figure S1A**). The quantitative explanation of this phenomenon lies prevalently in (i) an enhancement of the specific interactions of the

aromatic ring with Y120, F133, H154, and M170 in the related σ_1 receptor hydrophobic pocket ($\text{AVG}\Sigma\Delta H_{\text{RES}8\text{a}-11\text{a}} = -4.23$ kcal/mol, $\text{AVG}\Sigma\Delta H_{\text{RES}8\text{b}-11\text{b}} = -4.71$ kcal/mol, $\text{AVG}\Sigma\Delta H_{\text{RE}13\text{a}-16\text{a}} = -3.81$ kcal/mol, and $\text{AVG}\Sigma\Delta H_{\text{MD}13\text{b}-16\text{b}} = -4.2$ kcal/mol, **Figure S1B**) and (ii) an optimization of the fundamental salt bridge with the negatively charged side chain of E172 in molecules in which the N-atom is enclosed in the piperidine ring ($\text{AVG}\Sigma\Delta H_{\text{RES}8\text{a}-11\text{a}} = -4.60$ kcal/mol, $\text{AVG}\Sigma\Delta H_{\text{RES}8\text{b}-11\text{b}} = -5.27$ kcal/mol, $\text{AVG}\Sigma\Delta H_{\text{RE}13\text{a}-16\text{a}} = -4.41$ kcal/mol, and $\text{AVG}\Sigma\Delta H_{\text{MD}13\text{b}-16\text{b}} = -4.64$ kcal/mol, **Figure S1B**).

Our computational analysis concludes with the aim to rationalize the pronounced selectivity of the new derivatives toward the σ_1 receptor over the σ_2 and NMDA receptors. For

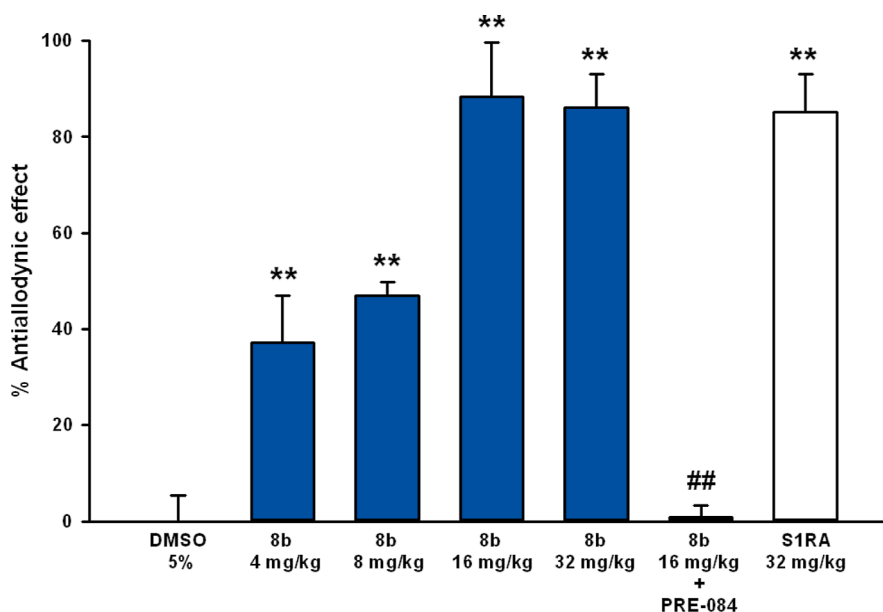


Figure 4. Antiallodynic activity of aminodiol **8b**. Female CD-1 mice were intraplantarly injected with capsaicin to induce tactile allodynia. DMSO served as a negative control and the prototypical σ_1 antagonist S1RA (32 mg kg⁻¹, s.c.) as a positive control. **8b** was administered subcutaneously (s.c.) at doses of 4, 8, 16, and 32 mg kg⁻¹. The antiallodynic effect of **8b** (16 mg kg⁻¹, s.c.) was abolished by the σ_1 agonist PRE-084 (32 mg kg⁻¹, s.c.). ** $p < 0.01$ significant differences compared with the negative control 5% DMSO; ## $p < 0.01$ significant differences compared with **8b** (16 mg kg⁻¹). One-way analysis of variance (ANOVA), followed by the Bonferroni test.

this purpose, the same computational approach was applied to study the **10b**/ σ_2 and **10b**/NMDA complexes (Figure 3). MM/PBSA analysis yielded ΔG_{MD} values of -8.88 kcal/mol for the **10b**/ σ_2 complex and -9.10 kcal/mol for the **10b**/NMDA complex, both in line with the experimental lines of evidence. Moreover, the precise binding mechanism revealed by PRBFED analysis agrees with that previously described for ligands with chemical structures similar to **10b** toward the same biological targets.^{38–40}

Basically, **10b** is able to perform only one specific interaction within the corresponding binding pockets: a salt bridge with D29 in the σ_2 receptors and a permanent hydrogen bond with the amide group on the side chain of Q110 belonging to the GluN2B subunit of the NMDA dimer. The other moieties of the **10b** structure can be appropriately encased into the hydrophobic cavities of the σ_2 receptor or into the dimeric interface between the subunits GluN1b and GluN2B of the NMDA receptor (Figure 3). In this case, however, punctual interactions are not detected but, mostly, generic stabilizing hydrophobic interactions (Figure 3).

2.7. In Vitro ADME Characterization. The lipophilicity influences the pharmacokinetic properties of drug candidates. High lipophilicity (high $\log D$ value) can result in low solubility and rapid metabolism, whereas low lipophilicity (low $\log D$ value) may lead to low cell permeability and fast renal elimination. Optimal $\log D$ values range from 1 or 1.5 to 3.^{41,42}

Hence, the $\log D$ values of five prototypical compounds of this series at physiological pH value 7.4 ($\log D_{7.4}$) were determined experimentally. For this purpose, the recently published micro shake flask method^{43,44} was used. In this assay, the σ_1 ligands were distributed between an *n*-octanol and a MOPS buffer pH 7.4 layer. The amount of ligand in the aqueous layer was determined by mass spectrometry.

To evaluate the influence of structural features on lipophilicity, the stereochemistry was kept constant, i.e., the $\log D_{7.4}$ value of the (*R,R,R,R,R*)-configured stereoisomer of

each series was determined. Aminodiol **8a** with the 4-phenylbutyl substituent showed the lowest $\log D_{7.4}$ value of 1.84 (Table 2), as it combines most H-bond donor groups with least aliphatic C-atoms. Removal of two H-bond donor groups by introduction of a methylene bridge between the O-atoms led to the bicyclic acetal **13a** with increased lipophilicity ($\Delta \log D_{7.4} = +0.83$). Rigidization of the 4-phenylbutyl side chain of **8a** by addition of an ethylene bridge resulted in benzylpiperidine **8b** with further increased lipophilicity ($\Delta \log D_{7.4} = +1.21$). The combination of both variations in **13b** increased the $\log D_{7.4}$ value additively to 3.45 ($\Delta \log D_{7.4} = +1.61$). The tricyclic ligand **19** displays the highest lipophilicity ($\log D_{7.4} = 3.96$). This is probably due to the increased rigidity which limits the interaction of the amino group with polar solvents such as water.

The affinity of a ligand to a biological target usually increases with the introduction of lipophilic structural elements, leading to unspecific lipophilic interactions which increase the entropic contribution to the binding. Therefore, the LLE index correlating binding affinity values with lipophilicity should be taken into account. LLE is the ratio between drug potency, e.g., K_i value, and calculated $c \log P$ or $\log D$ value.^{45,46} In this study, experimentally determined $\log D_{7.4}$ values were used instead of calculated $c \log P$ or $\log D$ values to calculate the LLE. Drug candidates should have a LLE index >5 .

The bicyclic benzylpiperidine **13b** has slightly higher σ_1 affinity, but increased lipophilicity than the aminodiol **8a**, which results in reduced LLE. The lower σ_1 affinity and moderate lipophilicity of **13a** reduced its LLE index, whereas the high σ_1 affinity of **8b** resulted in a promising LLE index of 5.87.

To determine the plasma protein binding (PPB), a high-performance affinity chromatography (HPAC) using a stationary phase coated with human serum albumin was performed. The retention on this column correlates with the affinity of a ligand toward human serum albumin, which is the

most abundant protein in the plasma. The aminodiol **8b** with the benzylpiperidino moiety exhibited the lowest PPB of 87.8%, whereas **8a**, **13a**, and **13b** had similar PPBs of around 93%. The tricyclic ligand **19** with the lowest σ_1 affinity, the highest lipophilicity, and the lowest LLE index was almost completely bound to the human serum albumin (PPB >98%).

Due to the high σ_1 affinity ($K_i = 1.2$ nM) and promising LLE index of 5.87, we planned to test the analgesic activity of **8b** in vivo. For the preparation of the in vivo tests, the metabolic stability was tested by incubation of **8b** with mouse liver microsomes and NADPH. After an incubation period of 90 min, 19% of **8b** remained intact, which indicated only moderate metabolic stability.

2.8. Antiallodynic Activity of 8b. Allodynia is characterized by a hypersensitive reaction to normal mechanical stimuli. It was induced in mice by injection of capsaicin into the hind paw. After the initial pain (acute pain) had subsided, the remaining allodynia was determined by touching the hind paw with a von Frey filament. It has been reported that σ_1 -knockout mice do not develop significant capsaicin-induced allodynia.¹⁸ Moreover, σ_1 receptor agonists enhance⁴⁷ and σ_1 receptor antagonists inhibit¹⁸ capsaicin-induced allodynia. Thus, the antiallodynic activity of the aminodiol **8b** displaying very high σ_1 receptor affinity ($K_i = 1.2$ nM) was tested in the capsaicin-induced allodynia assay in vivo in mice (Figure 4).

To evaluate the antiallodynic activity of aminodiol **8b**, female CD-1 mice were injected with either the test compound or DMSO as a negative control. After 30 min, capsaicin was injected into the hind paw to induce tactile allodynia. After 15 min, a von Frey filament stimulated the paw. **8b** increased the latency of paw withdrawal at doses from 32 mg kg⁻¹ to as low as 4 mg kg⁻¹ (Figure 4). The treatment with the prototypical σ_1 receptor antagonist SIRA (32 mg kg⁻¹) displayed similar results to treatment with the highest doses of **8b** used (16 and 32 mg kg⁻¹). Injection of the σ_1 receptor agonist PRE-084 (32 mg kg⁻¹) before application of **8b** (16 mg kg⁻¹) reduced the antiallodynic effect of **8b** considerably. This competition experiment proves that inhibition of σ_1 receptors is responsible for the antiallodynic activity of **8b** showing similar effects of the well-known σ_1 receptor antagonist SIRA. Hence, **8b** represents a potent σ_1 receptor antagonist with high antiallodynic activity.

At a dose of 16 mg kg⁻¹, the antiallodynic activity of **8b** is higher than the antiallodynic activity of prototypical σ_1 ligands SIRA and BD-1063, and the ED₅₀ value of **8b** is considerably lower than the ED₅₀ value of SIRA and BD-1063 (Table 3). Thus, it can be concluded that aminodiol **8b** is a high-affinity σ_1 receptor antagonist with a promising LLE index and high antiallodynic activity.

3. CONCLUSIONS

σ_1 Receptor antagonists are promising candidates for the treatment of various types of pain. Starting from the monoterpenoid (–)-isopulegol (**1**), a series of potent and subtype-selective σ_1 receptor ligands was prepared. As the first key feature, the configuration of two centers of chirality was systematically varied, i.e., four stereoisomers were produced for each structural motif. As the second key feature, the rigidity of the ligand was systematically increased: the first subgroup contains aminodiols **8a–11a** bearing the rather flexible 4-phenylbutylamino substituent. Introduction of an ethylene bridge into this side chain resulted in the 4-benzylpiperidino series **8b–11b**, and connecting the two OH moieties by

Table 3. Comparison of the Antiallodynic Activity of 8b with Standard σ_1 Antagonists SIRA and BD-1063 at a Dose of 16 mg kg⁻¹ Body Weight in the Capsaicin-Induced Allodynia Test

| compd. | antiallodynic activity (16 mg kg ⁻¹ body weight) (%) | ED ₅₀ [mg kg ⁻¹] |
|---|---|---|
| 8b (s.c.) | ~89 | ~8 ^a |
| SIRA ²¹ (i.p.) ^b | 43 ⁴⁸ | 26.3 ± 5.5 ⁴⁸ |
| BD-1063 ⁴¹ (s.c.) ^c | ~3 ⁵⁰ | ~40 ⁵⁰ |

^aThe ED₅₀ value of **8b** was estimated from the activity displayed in Figure 4. ^bThe antiallodynic activity at a dose of 16 mg kg⁻¹ was estimated. Note that the antiallodynic activity was evaluated 15 min after capsaicin administration in male mice. ^cThe ED₅₀ value and the antiallodynic activity of BD-1063 were estimated from the literature data.^{49,50} The antiallodynic activity was evaluated following the same experimental conditions as in the present study.

formation of a formaldehyde acetal led to the bicyclic compounds **13–16**. Connecting the N-atom with the methylene moiety of the formaldehyde acetal finally gave the highest level of rigidization in compounds **19–22** with a tricyclic scaffold. High σ_1 affinity ($K_i = 1.0–69$ nM) was found for the rather polar aminodiols **8–11** and their more rigid and less polar bicyclic analogues **13–16**. The tricyclic analogues **19–22** showed considerably lower σ_1 affinity. Stereoisomers **8** and **10** with (*R*)-configuration in the aminohydroxypropan-2-yl side chain displayed higher σ_1 affinity than their diastereomers **9** and **11** with (*S*)-configuration. Benzylpiperidino derivatives (**b**-series) exhibited higher σ_1 affinity than 4-phenylbutyl-substituted secondary amines (**a**-series). Compounds with high σ_1 affinity demonstrated high selectivity over related σ_2 receptors and the ifenprodil binding site of NMDA receptors.

According to MD simulations, all compounds adopt similar binding poses at the σ_1 receptor binding site. The hydroxy groups of the aminodiols **8–11** appeared to be not crucial for σ_1 receptor binding since only weak polar interactions with the side chain of T181 were observed. The MD simulations confirmed the low impact of the absolute configuration on the interactions with the σ_1 receptor. On the contrary, the protonated amino moiety performs the most important polar interactions, i.e., a π -cation interaction with the aromatic side chain of F107 and an ionic interaction with E172. The enthalpic contribution is responsible for the different affinities of aminodiols and bicyclic and tricyclic analogues, which cannot be compensated by entropic factors. Compounds with a piperidine spacer (**b**-series) instead of a butylamine spacer (**a**-series) exhibited a gain of about 1 kcal/mol on the ΔG_{MD} values, which was explained by enhanced specific interactions of the terminal phenyl moiety and the optimal orientation of the salt bridge. MD simulations of the interactions of **10b** with σ_2 receptors and the ifenprodil binding site of the NMDA receptor were able to rationalize its selectivity over these targets.

To select a σ_1 ligand for in vivo studies, in vitro ADME parameters were recorded. The aminodiol **8b** with the 4-benzylpiperidino moiety showed very high σ_1 affinity ($K_i = 1.2$ nM), moderate lipophilicity ($\log D_{7.4} = 3.05$), promising LLE (5.87), and the lowest PPB (PPB = 87%) this series of ligands. Moreover, incubation with mouse liver microsomes and NADPH for 90 min resulted in moderate metabolic stability.

In the capsaicin-mediated antiallodynia assay, **8b** showed high antiallodynic activity. At a dose of 8 mg kg⁻¹ body weight, almost 50% efficacy was observed. Removal of the antiallodynic activity of **8b** by co-application of the σ_1 agonist PRE-084 confirmed that the antiallodynic activity of **8b** is based on the inhibition of σ_1 receptors. The antiallodynic activity of **8b** is similar to the antiallodynic activity of prototypical σ_1 antagonists S1RA and BD-1063.

4. EXPERIMENTAL SECTION

4.1. Chemistry, General. Unless otherwise noted, moisture-sensitive reactions were conducted under dry nitrogen. CH₂Cl₂ was distilled over CaH₂. THF and toluene were distilled over sodium/benzophenone. All other solvents were dried over molecular sieve 0.4, or 0.3 Å, when applicable. Thin-layer chromatography (tlc): silica gel 60 F254 plates (Merck). fc: silica gel 60, 40–64 μm (Merck). Melting point: melting point apparatus Mettler Toledo MP50 Melting Point System, uncorrected. MS: microTOF-Q II (Bruker Daltonics); APCI, atmospheric pressure chemical ionization. IR: FT-IR spectrophotometer MIRacle 10 (Shimadzu) equipped with ATR technique. NMR spectra were recorded on an Agilent 600 MR (600 MHz for ¹H and 151 MHz for ¹³C) or an Agilent 400 MR spectrometer (400 MHz for ¹H and 101 MHz for ¹³C); δ in ppm related to tetramethylsilane and measured referring to CHCl₃ (δ = 7.26 ppm (¹H NMR) and δ = 77.2 ppm (¹³C NMR)), CHD₂OD (δ = 3.31 ppm [¹H NMR] and δ = 49.0 ppm [¹³C NMR]) and DMSO-*d*₆ [δ = 2.54 ppm (¹H NMR) and δ = 39.5 ppm (¹³C NMR)]; coupling constants are given with 0.5 Hz resolution; the assignments of ¹³C and ¹H NMR signals were supported by 2-D NMR techniques where necessary.

4.2. HPLC Equipment and Methods. HPLC method 1 to determine the purity of compounds: Pump: LPG-3400SD, degasser: DG-1210, autosampler: ACC-3000T, UV detector: VWD-3400RS, interface: DIONEX UltiMate 3000, and data acquisition: Chromeleon 7 (Thermo Fisher Scientific); column: LiChropher 60 RP-select B (5 μm), LiChroCART 250–4 mm cartridge; flow rate: 1.0 mL/min; injection volume: 5.0 μL; detection at λ = 210 nm; solvents A: demineralized water with 0.05% (V/V) trifluoroacetic acid; solvent B: acetonitrile with 0.05% (V/V) trifluoroacetic acid; and gradient elution (% A): 0–4 min: 90%; 4–29 min: gradient from 90 to 0%; 29–31 min: 0%; 31–31.5 min: gradient from 0 to 90%; and 31.5–40 min: 90%.

HPLC method 2: Pump: L-7100, degasser: L-7614, autosampler: L-7200, UV detector: L-7400, interface: D-7000, data transfer: D-line, and data acquisition: HSM-Software (all from LaChrom, Merck Hitachi); column: Phenomenex Gemini C18 110 Å, size: 250 × 4.60 mm (5 μm); flow rate: 1.0 mL/min; injection volume: 10.0 μL; detection at λ = 210 nm; solvent A: demineralized water with 0.05% (V/V) NH₃, solvent B: acetonitrile with 0.05% (V/V) NH₃; and gradient elution (% A): 0–4 min: 90%; 4–29 min: gradient from 90 to 0%; 29–33 min: 0%; 33–33.5 min: gradient from 0 to 90%; and 33.5–40 min: 90%. The purity of all test compounds is greater than 95%, unless otherwise noted.

4.3. Synthetic Procedures. (–)-*trans*-Isopulegone (**2**),⁵¹ (+)-neoisopulegol (**3**),²⁴ and epoxides **4/5**^{52,53} and **7**²⁴ have been synthesized as previously described.

4.3.1. (1*R*,2*R*,5*R*)-2-[(*R*)-1-(4-phenylbutyl)amino]propan-2-yl]-5-methylcyclohexan-1-ol (8a**) and (1*R*,2*R*,5*R*)-2-[(*S*)-2-Hydroxy-1-(4-phenylbutyl)amino]propan-2-yl]-5-methylcyclohexan-1-ol (**9a**).** The mixture of epoxides **4** and **5** (ca. 1:1, 1.00 g, 5.87 mmol, 1.00 equiv) and 4-phenylbutylamine (927 mg, 6.21 mmol, 1.06 equiv) were dissolved in CH₃OH (10 mL). The reaction mixture was stirred under reflux for 22 h. The solvent was removed. The crude product was purified by flash column chromatography (cyclohexane/EtOAc 3:7 + 1% *N,N*-dimethylethylamine) to yield a mixture of **8a** and **9a** (**8a:9a** = 58:42, 1.39 g, 4.35 mmol, 74%). Flash column chromatography (cyclohexane/EtOAc 2:1 + 1% *N,N*-dimethylethylamine) yielded **8a** (319 mg, 17%), a mixture of **8a** and **9a** (**8a:9a** = 51:49, 933 mg, 50%) and **9a** (80 mg, 4%).

8a: Colorless oil, yield 319 mg (17%), C₂₀H₃₃NO₂ (319.5 g mol⁻¹). R_f = 0.42 (CH₂Cl₂/CH₃OH 10:1 + 1% NH₃). Purity (HPLC, method 1): 97.4% (t_R = 17.3 min). HR-MS (APCI): m/z = 320.2577, calcd 320.2584 for C₂₀H₃₄NO₂⁺ [M + H]⁺. IR: $\hat{\nu}$ [cm⁻¹] = 3310 (O–H, N–H), 2920 (C–H_{aliph}), 1454 (C–H_{aliph}), 1049 (C–O), 745 (C–H_{arom}), 698 (C–H_{arom}). Specific rotation: $[\alpha]_{20}^D$ = +12.9 (c = 0.43, CH₂Cl₂). ¹H NMR (600 MHz, CDCl₃): δ [ppm] = 0.87 (qd, J = 12.9/3.0 Hz, 1H, 4-*H*_{ax}), 0.91 (d, J = 6.5 Hz, 1H, 5-*CH*₃), 0.94 (qd, J = 12.7/3.1 Hz, 1H, 3-*H*_{ax}), 1.00 (td, J = 12.3/10.7 Hz, 1H, 6-*H*_{ax}), 1.14 (s, 3H, 2-*CCH*₃), 1.34 (ddd, J = 12.1/9.8/3.5 Hz, 1H, 2-*H*), 1.42 (tqt, J = 11.9/6.7/3.5 Hz, 1H, 5-*H*), 1.51 (quint, J = 7.5 Hz, 2H, NCH₂CH₂), 1.56 (dq, J = 12.4/3.1 Hz, 1H, 3-*H*_{eq}), 1.61–1.69 (m, 3H, 4-*H*_{eq}, CH₂CH₂Ph), 1.96 (dtd, J = 12.5/4.0/2.0 Hz, 1H, 6-*H*_{eq}), 2.41 (d, J = 12.3 Hz, 1H, 2-*CCH*₂N), 2.60–2.68 (m, 4H, NCH₂CH₂CH₂CH₂Ph), 2.68 (d, J = 12.3 Hz, 1H, 2-*CCH*₂N), 3.73 (ddd, J = 10.7/9.7/4.3 Hz, 1H, 1-*H*), 7.16–7.20 (m, 3H, 2-*H*_{aryl}, 4-*H*_{aryl}, 6-*H*_{aryl}), 7.26–7.30 (m, 2H, 3-*H*_{aryl}, 5-*H*_{aryl}). Signals for the OH and NH protons are not observed in the spectrum. ¹³C NMR (151 MHz, CDCl₃): δ [ppm] = 22.2 (1C, 5-*CH*₃), 26.2 (1C, C-3), 26.5 (1C, 2-*CCH*₃), 29.1 (1C, CH₂CH₂Ph), 29.9 (1C, NCH₂CH₂), 31.5 (1C, C-5), 34.9 (1C, C-4), 35.9 (1C, CH₂Ph), 44.3 (1C, C-6), 50.5 (1C, NCH₂CH₂), 52.8 (1C, C-2), 54.8 (1C, 2-*CCH*₂N), 71.8 (1C, C-1), 75.0 (1C, H₃CCOH), 125.9 (1C, C-4_{aryl}), 128.5 (2C, C-3_{aryl}, C-5_{aryl}), 128.5 (2C, C-2_{aryl}, C-6_{aryl}), 142.4 (1C, C-1_{aryl}).

9a: Colorless solid, mp 50 °C, yield 80 mg (4%). C₂₀H₃₃NO₂ (319.5 g mol⁻¹). R_f = 0.37 (CH₂Cl₂:CH₃OH 10:1 + 1% NH₃). Purity (HPLC, method 1): 92.5% (t_R = 17.09 min). HR-MS (APCI): m/z = 320.2571 (calcd 320.2584 for C₂₀H₃₄NO₂⁺ [M + H]⁺). IR: $\hat{\nu}$ [cm⁻¹] = 3244 (O–H, N–H), 2909 (C–H_{aliph}), 1111 (C–H_{alcohol} C–O), 1049 (C–O), 748 (C–H_{arom}), 694 (C–H_{aliph}). Specific rotation: $[\alpha]_{20}^D$ = +13.4 (c = 0.16, CH₂Cl₂). ¹H NMR (600 MHz, CDCl₃): δ [ppm] = 0.88 (qd, J = 12.5/2.9 Hz, 1H, 4-*H*_{ax}), 0.92 (d, J = 6.5 Hz, 3H, 5-*CH*₃), 0.97 (qd, J = 12.7/3.1 Hz, 1H, 3-*H*_{ax}), 1.02 (td, J = 12.4/10.8 Hz, 1H, 6-*H*_{ax}), 1.14 (s, 3H, 2-*CCH*₃), 1.37–1.46 (m, 1H, 5-*H*), 1.48–1.56 (m, 3H, 2-*H*, NCH₂CH₂), 1.63–1.68 (m, 3H, 4-*H*_{eq}, CH₂CH₂Ph), 1.70 (dq, J = 12.9/3.4 Hz, 1H, 3-*H*_{eq}), 1.96 (dtd, J = 12.5/3.9/2.0 Hz, 1H, 6-*H*_{eq}), 2.60–2.66 (m, 5H, CH₂NHCH₂CH₂CH₂CH₂Ph), 2.72 (dt, J = 11.7/7.1 Hz, 1H, NCH₂CH₂), 3.61 (td, J = 10.4/4.3 Hz, 1H, 1-*H*), 7.15–7.20 (m, 3H, 2-*H*_{aryl}, 4-*H*_{aryl}, 6-*H*_{aryl}), 7.26–7.30 (m, 2H, 3-*H*_{aryl}, 5-*H*_{aryl}). Signals for the NH and OH protons were not seen in the spectrum. ¹³C NMR (151 MHz, CDCl₃): δ [ppm] = 22.2 (1C, 5-*CH*₃), 26.2 (1C, C-3), 26.5 (1C, 2-*CCH*₃), 29.1 (1C, CH₂CH₂Ph), 29.9 (1C, NCH₂CH₂), 31.5 (1C, C-5), 34.9 (1C, C-4), 35.9 (1C, CH₂Ph), 44.3 (1C, C-6), 50.5 (1C, NCH₂CH₂), 52.8 (1C, C-2), 54.8 (1C, 2-*CCH*₂N), 71.8 (1C, C-1), 75.0 (1C, 2-*CCH*₃), 125.9 (1C, C-4_{aryl}), 128.5 (2C, C-3_{aryl}, C-5_{aryl}), 128.5 (2C, C-2_{aryl}, C-6_{aryl}), 142.4 (1C, C-1_{aryl}).

4.3.2. (1*R*,2*R*,5*R*)-2-[(*R*)-1-(4-Benzylpiperidin-1-yl)-2-hydroxypropan-2-yl]-5-methylcyclohexan-1-ol (8b**) and (1*R*,2*R*,5*R*)-2-[(*S*)-1-(4-Benzylpiperidin-1-yl)-2-hydroxypropan-2-yl]-5-methylcyclohexan-1-ol (**9b**).** The mixture of epoxides **4** and **5** (ca. 1:1, 700 mg, 4.11 mmol, 1.00 equiv) and benzylpiperidine (937 mg, 5.35 mmol, 1.30 equiv) were dissolved in CH₃OH (80 mL). The reaction mixture was stirred under reflux for 40 h. The solvent was removed in vacuo. The crude product was purified by column chromatography (cyclohexane/ethyl acetate 5:1 + 1% *N,N*-dimethylethylamine, then cyclohexane/ethyl acetate 1:1 + 1% *N,N*-dimethylethylamine). **8b:9b**: Orange oil, yield 1.31 g (92%), **8b:9b** = 56:44. The mixture of **8b** and **9b** (747 mg) was separated by HPLC (Phenomenex Lux Cellulose-2 (250 × 21.1 mm, 5 μm), 100 mL min⁻¹, gradient CO₂:CH₃OH 20:1 + 20 mM NH₃ → CO₂/CH₃OH 1:1 + 20 mM NH₃).

8b: Yellow oil, yield 350 mg (43%). C₂₂H₃₅NO₂ (345.5 g mol⁻¹). R_f = 0.45 (cyclohexane/EtOAc 1:1 + 1% *N,N*-dimethylethylamine). Purity (HPLC, method 2): 100% (t_R = 3.97 min). HR-MS (APCI): m/z = 346.2803, calcd 346.2741 for C₂₂H₃₆NO₂ [M + H]⁺. IR: $\hat{\nu}$ [cm⁻¹] = 3333 (O–H), 2916 (C–H_{aliph}), 1450 (C–H_{aliph}), 1049 (C–O), 698 (C–H_{arom}). Specific rotation: $[\alpha]_{20}^D$ = +5.2 (c = 0.48, CH₂Cl₂). ¹H NMR (600 MHz, CD₃OD): δ [ppm] = 0.89 (qd, J = 13.0/3.0 Hz, 1H, 4-*H*_{ax}), 0.93 (d, J = 6.6 Hz, 3H, 5-*CH*₃), 0.97 (qd, J

equiv), and bromoacetaldehyde dimethyl acetal (53 mg, 0.31 mmol, 2.1 equiv) were dissolved in DMF (1 mL). The reaction mixture was stirred at 130 °C for 20 h. After cooling to rt, H₂O (10 mL) was added, and the reaction mixture was extracted with CH₂Cl₂ (5 × 5 mL). The combined organic layers were washed with brine (5 mL) and dried (Na₂SO₄). Residual DMF was co-evaporated with toluene (5 × 5 mL). The crude intermediate **25** was dissolved in CHCl₃ (10 mL). *p*-Toluenesulfonic acid monohydrate (60 mg, 0.31 mmol, 2.1 equiv) was added, and the reaction mixture was stirred at 80 °C for 1.5 h. After cooling to rt, the reaction was terminated by addition of Na₂CO₃ (1 mL). The aqueous layer was extracted with CH₂Cl₂ (3 × 3 mL). The combined organic layers were washed with brine (3 mL) and dried (Na₂SO₄). The crude product was purified by flash column chromatography (cyclohexane/ethyl acetate 40:1 + 1% *N,N*-dimethylethylamine). Pale yellow oil, yield 10 mg (19%). C₂₂H₃₃NO₂ (343.5 g mol⁻¹). R_f = 0.45 (cyclohexane/EtOAc 9:1 + 1% *N,N*-dimethylethylamine). Purity (HPLC, method 1): 92.3% (t_R = 19.2 min). HR-MS (APCI): *m/z* = 344.2553, calcd 344.2584 for C₂₂H₃₄NO₂⁺ [M + H]⁺. IR: ν̄ [cm⁻¹] = 2928 (C–H_{aliph}), 2859 (C–H_{aliph}), 1454 (C–H_{aliph}), 1142 (C–O), 1049 (C–O, C–N), 745 (C–H_{arom}), 698 (C–H_{arom}). Specific rotation: [α]₂₀^D = +11.8 (c = 0.14, CH₂Cl₂). ¹H NMR (600 MHz, CDCl₃): δ [ppm] = 0.91 (q, *J* = 11.6 Hz, 1H, 4-H_{ax}), 0.92 (d, *J* = 6.6 Hz, 3H, 5-CH₃), 0.97 (qd, *J* = 12.8/3.8 Hz, 1H, 6-H_{ax}), 1.08 (qd, *J* = 12.6/3.5 Hz, 1H, 7-H_{ax}), 1.11 (s, 3H, 9-CH₃), 1.43–1.53 (m, 4H, NCH₂CH₂, 5-H, 8-H), 1.62 (dq, *J* = 12.7/3.4 Hz, 1H, 7-H_{eq}), 1.65–1.74 (m, 3H, 6-H_{eq}, CH₂CH₂Ph), 1.85 (dtd, *J* = 11.7/3.7/1.7 Hz, 1H, 4-H_{eq}), 2.04 (dd, *J* = 11.5/1.6 Hz, 1H, 10-H_{ax}), 2.18 (dt, *J* = 12.0/6.7 Hz, 1H, NCH₂CH₂), 2.25 (dt, *J* = 12.0/7.1 Hz, 1H, NCH₂CH₂), 2.35 (dd, *J* = 11.5/2.9 Hz, 1H, 12-H_{ax}), 2.61 (dt, *J* = 13.9/7.4 Hz, 1H, CH₂Ph), 2.64 (dt, *J* = 13.9/7.4 Hz, 1H, CH₂Ph), 2.88 (d, *J* = 11.4 Hz, 1H, 10-H_{eq}), 3.00 (d, *J* = 11.4 Hz, 1H, 12-H_{eq}), 5.04 (td, *J* = 10.6/3.5 Hz, 1H, 3-H), 5.05–5.07 (m, 1H, 1-H), 7.16–7.20 (m, 3H, 2-H_{aryl}, 4-H_{aryl}, 6-H_{aryl}), 7.26–7.30 (m, 2H, 3-H_{aryl}, 5-H_{aryl}). ¹³C NMR (151 MHz, CDCl₃): δ [ppm] = 22.4 (1C, 5-CH₃), 25.6 (1C, C-7), 25.7 (1C, 9-CH₃), 26.1 (1C, CH₂CH₂Ph), 29.4 (1C, NCH₂CH₂), 31.6 (1C, C-5), 35.3 (1C, C-6), 35.8 (1C, CH₂Ph), 42.3 (1C, C-4), 51.8 (1C, C-8), 56.8 (1C, C-12), 58.2 (1C, C-10), 58.3 (1C, NCH₂CH₂), 72.6 (1C, C-9), 74.5 (1C, C-3), 93.2 (1C, C-1), 125.9 (1C, C-4_{aryl}), 128.4 (2C, C-3_{aryl}, C-5_{aryl}), 128.5 (2C, C-2_{aryl}, C-6_{aryl}), 142.7 (1C, C-1_{aryl}).

4.3.21. (1*S*,3*S*,5*R*,8*R*,9*R*)-5,9-Dimethyl-11-(4-phenylbutyl)-2,13-dioxo-11-azatricyclo[7.3.1.0^{3,8}]tridecane (21). Aminodiol **10a** (77 mg, 0.24 mmol, 1.0 equiv), K₂CO₃ (66 mg, 0.48 mmol, 2.0 equiv), and bromoacetaldehyde dimethyl acetal (82 mg, 0.49 mmol, 2.0 equiv) were dissolved in DMF (1 mL). The reaction mixture was stirred at 130 °C for 22 h. After cooling to rt, H₂O (3 mL) was added, and the reaction mixture was extracted with CH₂Cl₂ (5 × 4 mL). The combined organic layers were washed with brine (3 mL) and dried (Na₂SO₄). Residual DMF was co-evaporated with toluene (6 × 2 mL). The crude product (intermediate **26**) was dissolved in CHCl₃ (25 mL), and *p*-toluenesulfonic acid monohydrate (91 mg, 0.48 mmol, 2.0 equiv) was added. The reaction mixture was stirred at 80 °C for 3.5 h. After cooling to rt, Na₂CO₃ (4 mL) was added. The aqueous layer was extracted with CH₂Cl₂ (3 × 12 mL). The combined organic layers were washed with brine (12 mL), dried (Na₂SO₄), and concentrated in vacuo. The crude product was purified by flash column chromatography (cyclohexane/EtOAc 100:1 + 1% *N,N*-dimethylethylamine). Colorless oil, yield 27 mg (33%). C₂₂H₃₃NO₂ (343.5 g mol⁻¹). R_f = 0.48 (cyclohexane/EtOAc 10:1 + 1% *N,N*-dimethylethylamine). Purity (HPLC, method 1): 96.3% (t_R = 19.2 min). HR-MS (APCI): *m/z* = 344.2574, calcd 344.2584 for C₂₂H₃₄NO₂⁺ [M + H]⁺. IR: ν̄ [cm⁻¹] = 2939 (C–H_{aliph}), 1454 (C–H_{aliph}), 1111 (C–O), 745 (C–H_{arom}), 698 (C–H_{arom}). Specific rotation: [α]₂₀^D = –25.7 (c = 0.22, CH₂Cl₂). ¹H NMR (600 MHz, CDCl₃): δ [ppm] = 0.85 (d, *J* = 6.6 Hz, 3H, 5-CH₃), 0.86 (qd, *J* = 13.0/3.4 Hz, 1H, 6-H_{ax}), 1.04 (ddd, *J* = 14.5/12.4/3.5 Hz, 1H, 4-H_{ax}), 1.06 (s, 3H, 9-CH₃), 1.34 (dt, *J* = 12.3/4.0 Hz, 1H, 8-H), 1.50 (quint, *J* = 7.0 Hz, 2H, NCH₂CH₂), (dq, *J* = 12.5/4.1 Hz, 1H, 7-H_{eq}), 1.61–1.70 (m, 3H, 5-H, CH₂CH₂Ph), 1.72 (dq, *J* = 13.0/3.4 Hz, 1H, 6-H_{eq}), 1.77–1.86 (m, 2H, 4-H_{eq}, 7-H_{ax}), 2.18 (dt, *J* = 12.1/7.3 Hz, 1H,

NCH₂CH₂), 2.20 (t, *J* = 12.1/7.3 Hz, 1H, NCH₂CH₂), 2.21 (d, *J* = 11.7 Hz, 1H, 10-H_{ax}), 2.30 (dd, *J* = 11.3/2.6 Hz, 1H, 12-H_{ax}), 2.62 (t, *J* = 14.0/7.9 Hz, 1H, CH₂Ph), 2.62 (t, *J* = 14.0/7.9 Hz, 1H, CH₂Ph), 2.86 (d, *J* = 11.3 Hz, 1H, 10-H_{eq}), 2.99 (dd, *J* = 11.2/1.2 Hz, 1H, 12-H_{eq}), 5.03–5.05 (t, *J* = 1.8 Hz, 1H, 1-H), 5.81 (q, *J* = 3.3 Hz, 1H, 3-H), 7.16–7.20 (m, 3H, 2-H_{aryl}, 4-H_{aryl}, 6-H_{aryl}), 7.26–7.30 (m, 2H, 3-H_{aryl}, 5-H_{aryl}). ¹³C NMR (151 MHz, CDCl₃): δ [ppm] = 22.5 (1C, 5-CH₃), 23.1 (1C, C-7), 24.9 (1C, 9-CH₃), 25.8 (1C, C-5), 26.0 (1C, NCH₂CH₂), 29.2 (1C, CH₂CH₂Ph), 34.5 (1C, C-6), 35.8 (1C, CH₂Ph), 40.7 (1C, C-4), 41.9 (1C, C-8), 56.7 (1C, C-12), 58.6 (1C, NCH₂CH₂), 63.8 (1C, C-10), 70.2 (1C, C-3), 71.8 (1C, C-9), 93.4 (1C, C-1), 125.8 (1C, C-4_{aryl}), 128.4 (2C, C-3_{aryl}, C-5_{aryl}), 128.5 (2C, C-2_{aryl}, C-6_{aryl}), 142.7 (1C, C-1_{aryl}).

4.3.22. (1*S*,3*S*,5*R*,8*R*,9*S*)-5,9-Dimethyl-11-(4-phenylbutyl)-2,13-dioxo-11-azatricyclo[7.3.1.0^{3,8}]tridecane (22). Aminodiol **11a** (100 mg, 313 μmol, 1.00 equiv) and *p*-toluenesulfonic acid monohydrate (77 mg, 0.41 mmol, 1.3 equiv) were dissolved in CHCl₃ (1 mL). Bromoacetaldehyde dimethyl acetal (58 mg, 0.34 mmol, 1.1 equiv) was added. The reaction mixture was stirred at 50 °C for 16 h (intermediate **27**). After cooling to rt, diisopropylethylamine (81 mg, 0.63 mmol, 2.0 equiv) and CHCl₃ (4 mL) were added. The reaction mixture was stirred at 60 °C for 96 h. Na₂CO₃ (4 mL) and CH₂Cl₂ (4 mL) were added. The aqueous layer was extracted with CH₂Cl₂ (2 × 4 mL). The combined organic layers were washed with water and brine (5 mL each) and dried (Na₂SO₄). The crude product was purified by flash column chromatography (cyclohexane + 1% *N,N*-dimethylethylamine). Pale yellow oil, yield 59 mg (55%). C₂₂H₃₃NO₂ (343.5 g mol⁻¹). R_f = 0.44 (cyclohexane/EtOAc 10:1 + 1% *N,N*-dimethylethylamine). Purity (HPLC, method 1): 97.4% (t_R = 19.8 min). HR-MS (APCI): *m/z* = 344.2563, calcd 344.2584 for C₂₂H₃₄NO₂⁺ [M + H]⁺. IR: ν̄ [cm⁻¹] = 2920 (C–H_{aliph}), 1454 (C–H_{aliph}), 1138 (C–O), 1045 (C–O), 745 (C–H_{arom}), 698 (C–H_{arom}). Specific rotation: [α]₂₀^D = +48.4 (c = 0.20, CH₂Cl₂). ¹H NMR (600 MHz, CDCl₃): δ [ppm] = 0.68–0.76 (qd, *J* = 12.6/3.0 Hz, 1H, 6-H_{ax}), 0.85 (d, *J* = 6.6 Hz, 3H, 5-CH₃), 1.13 (ddd, *J* = 14.4/12.5/4.2 Hz, 1H, 4-H_{ax}), 1.17 (s, 3H, 9-CH₃), 1.36 (ddd, *J* = 13.0/5.6/3.0 Hz, 1H, 7-H_{eq}), 1.43–1.71 (m, 6H, NCH₂CH₂CH₂Ph, 5-H, 6-H_{eq}), 1.74 (ddd, *J* = 12.4/5.6/3.9 Hz, 1H, 8-H), 1.86 (d, *J* = 11.5 Hz, 1H, 10-H_{ax}), 1.90 (dq, *J* = 14.5/2.7 Hz, 1H, 4-H_{eq}), 1.97 (dd, *J* = 11.1/1.5 Hz, 1H, 12-H_{ax}), 2.25 (dt, *J* = 12.1/7.3 Hz, 1H, NCH₂CH₂), 2.29 (dt, *J* = 12.1/7.3 Hz, 1H, NCH₂CH₂), 2.61 (t, *J* = 7.9 Hz, 2H, CH₂Ph), 2.67 (qd, *J* = 13.0/3.4 Hz, 1H, 7-H_{ax}), 2.71 (d, *J* = 11.6 Hz, 1H, 10-H_{eq}), 2.84 (dt, *J* = 11.1/1.5 Hz, 1H, 12-H_{eq}), 4.17 (q, *J* = 3.6 Hz, 1H, 3-H), 5.24 (t, *J* = 1.6 Hz, 1H, 1-H), 7.15–7.20 (m, 3H, 2-H_{aryl}, 4-H_{aryl}, 6-H_{aryl}), 7.25–7.29 (m, 2H, 3-H_{aryl}, 5-H_{aryl}). ¹³C NMR (151 MHz, CDCl₃): δ [ppm] = 24.8 (1C, C-7), 25.1 (1C, 5-CH₃), 28.6 (1C, NCH₂CH₂), 29.3 (1C, C-5), 31.6 (1C, 9-CH₃), 31.8 (1C, CH₂CH₂Ph), 36.6 (1C, C-6), 38.4 (1C, CH₂Ph), 41.6 (1C, C-4), 50.1 (1C, C-8), 58.1 (1C, C-12), 60.3 (1C, NCH₂CH₂), 62.6 (1C, C-10), 67.9 (1C, C-3), 75.1 (1C, C-9), 97.1 (1C, C-1), 128.2 (1C, C-4_{aryl}), 130.9 (2C, C-3_{aryl}, C-5_{aryl}), 131.0 (2C, C-2_{aryl}, C-6_{aryl}), 145.3 (1C, C-1_{aryl}).

4.4. Receptor Binding Studies. 4.4.1. General Procedures for the Binding Assays. The test compound solutions were prepared by dissolving approximately 10 μmol (usually 2–4 mg) of test compound in DMSO so that a 10 mM stock solution was obtained. To obtain the required test solutions for the assay, the DMSO stock solution was diluted with the respective assay buffer. The filtermats were presoaked in 0.5% aqueous polyethylenimine solution for 2 h at rt before use. All binding experiments were carried out in duplicates in the 96-well multiplates. The concentrations given are the final concentration in the assay. Generally, the assays were performed by addition of 50 μL of the respective assay buffer, 50 μL of the test compound solution in various concentrations (10⁻⁵, 10⁻⁶, 10⁻⁷, 10⁻⁸, 10⁻⁹, and 10⁻¹⁰ mol/L), 50 μL of the corresponding radioligand solution, and 50 μL of the respective receptor preparation into each well of the multiplate (total volume 200 μL). The receptor preparation was always added last. During the incubation, the multiplates were shaken at a speed of 500–600 rpm at the specified temperature. Unless otherwise noted, the assays were terminated after 120 min by rapid filtration using the

harvester. During the filtration, each well was washed five times with 300 μL of water. Subsequently, the filtermats were dried at 95 $^{\circ}\text{C}$. The solid scintillator was melted on the dried filtermats at a temperature of 95 $^{\circ}\text{C}$ for 5 min. After solidifying of the scintillator at rt, the trapped radioactivity in the filtermats was measured with the scintillation analyzer. Each position on the filtermat corresponding to one well of the multiplate was measured for 5 min with the [^3H]-counting protocol. The overall counting efficiency was 20%. The IC_{50} values were calculated with the program GraphPad Prism 3.0 (GraphPad Software, San Diego, CA, USA) by non-linear regression analysis. Subsequently, the IC_{50} values were transformed into K_i values using the equation of Cheng and Prusoff.⁵⁴ The K_i values are given as mean \pm SEM from three independent experiments.

4.4.2. σ_1 Receptor Assay.^{25–27} The assay was performed with the radioligand [^3H]-(+)-pentazocine (22.0 Ci/mmol; PerkinElmer). The thawed membrane preparation of guinea pig brain (about 100 μg of the protein) was incubated with various concentrations of test compounds, 2 nM [^3H]-(+)-pentazocine, and TRIS buffer (50 mM, pH 7.4) at 37 $^{\circ}\text{C}$. The non-specific binding was determined with 10 μM unlabeled (+)-pentazocine. The K_d value of (+)-pentazocine is 2.9 nM.⁵⁵

4.4.3. σ_2 Receptor Assay.^{25–27} The assays were performed with the radioligand [^3H]di-*o*-tolylguanidine (specific activity 50 Ci/mmol; ARC, St. Louis, MO, USA). The thawed rat liver membrane preparation (about 100 μg protein) was incubated with various concentrations of the test compound, 3 nM [^3H]di-*o*-tolylguanidine, and buffer containing (+)-pentazocine (500 nM (+)-pentazocine in TRIS buffer [50 mM TRIS, pH 8.0]) at rt. The non-specific binding was determined with 10 μM non-labeled di-*o*-tolylguanidine. The K_d value of di-*o*-tolylguanidine is 17.9 nM.⁵⁶

4.4.4. Ifenprodil Binding Site of the GluN2B Subunit Containing NMDA Receptors.²⁸ The competitive binding assay was performed with the radioligand [^3H]ifenprodil (60 Ci/mmol; BIOTREND, Cologne, Germany). The thawed cell membrane preparation from the transfected L(tk-) cells (about 20 μg protein) was incubated with various concentrations of test compounds, 5 nM [^3H]ifenprodil, and TRIS/EDTA buffer (5 mM TRIS/1 mM EDTA, pH 7.5) at 37 $^{\circ}\text{C}$. The non-specific binding was determined with 10 μM unlabeled ifenprodil. The K_d value of ifenprodil is 7.6 nM.²⁸

4.5. Computational Details. All simulations were carried out using Amber 20⁵⁷ running on our own CPU/GPU cluster. The starting molecular structures of the three receptors were obtained from the Protein Data Bank, specifically, PDB code 5HK1 for σ_1 receptor,³³ PDB code 7M96 for σ_2 receptor,³⁸ and PDB code 3QEM for the dimer of the NMDA receptor.⁵⁸ The entire modeling and simulation procedure is also reported in detail in earlier papers.^{34–36} Briefly, the geometry- and energy-optimized structure of all of the studied compounds was docked into each identified protein binding pocket using Autodock 4.2.6/Autodock Tools1.4⁵⁹ on a win64 platform. The resulting complexes were further energy-minimized to convergence. Each intermolecular complex was then solvated by a cubic box of TIP3P water molecules⁶⁰ and energy-minimized using a combination of MD techniques. 20 ns MD simulations at 298 K were then employed for system equilibration, and further, 50 ns MD simulations were run for data production. The binding free energies (ΔG_{MD}) were calculated following the MM/PBSA methodology⁶¹ as previously described.^{34–36} The PRBFED analysis was carried out using the molecular mechanics/generalized Boltzmann surface area approach,⁶² as already detailed^{34–36} and was based on the same snapshots used in the binding free energy calculation. Molecular graphics and analyses were performed with UCSF Chimera (v1.15).⁶³

4.6. Determination of Pharmacokinetic Parameters In Vitro.
4.6.1. Determination of $\log D_{7.4}$ Value.^{43,44}

4.6.1.1. Instruments and Parameters for LC–MS Standard Analysis. UPLC-UV/MS (Agilent Technologies): degasser: 1260 HiP (G4225A); pump: 1260 Bin Pump (G1212B); autosampler: 1260 HiP ALS (G1367E); column oven: 1290 TCC (G1316C), 30 $^{\circ}\text{C}$; UV/vis detector: 1260 VWD (G1314F); MS detector: 6120 Quadrupole LC/MS (G1978B); MS source: multimode source (G1978B); ESI mode; and SIM mode (m/z given for each compound). Data acquisition and settings were

performed with OpenLab CDS (ChemStation Edition, Agilent). Guard column: Zorbax Eclipse Plus-C18 (Agilent, Waldbronn, Germany) (2.1 mm \times 12.5 mm, 5.0 μm particle size). Main column: Zorbax SB-C18 (Agilent, Waldbronn, Germany) (2.1 mm \times 50 mm, 1.8 μm particle size). Spray chamber: vaporizer temperature: 200 $^{\circ}\text{C}$; drying gas: 12 L/min; nebulizer pressure: 40 psi; capillary voltage: 3000 V; corona current: 4 μA ; charging voltage: 2000 V; fragmentor voltage: 100 V; and drying gas temperature: 250 $^{\circ}\text{C}$. 2 mL safe lock tubes (Eppendorf) and 2 mL LC–MS vials (Agilent).

4.6.1.2. LC–MS Standard Method. Eluents: solvent A: $\text{H}_2\text{O}/\text{CH}_3\text{CN}$ 95:5 + 0.1% formic acid; solvent B: $\text{H}_2\text{O}/\text{CH}_3\text{CN}$ 5:95 + 0.1% formic acid; and gradient elution (A %): 0–2.5 min: gradient from 100 to 0%, 2.5–3.5 min: 0%, 3.5–4.0 min: gradient from 0 to 100%, and 4.0–8.0 min: 100%. Change valve position: after 1.0 min, the valve was switched from “waste” to “MS source”. Flow rate: 0.4 mL/min. Injection volume: 1.0 to 100 μL (given for each compound, 1.0 μL if not stated otherwise).

4.6.1.3. Chemicals, Solvents, and Stock Solutions. 3-Morpholinopropanesulfonic acid (MOPS) (Fisher Chemical, 372.5 mg, 8.9 mM) and MOPS sodium salt (Sigma-Aldrich, 513.4 mg, 11.1 mM) were dissolved in dist. H_2O (200 mL) to prepare a 20 mM buffer solution with pH 7.4. A mixture of *n*-octanol (Sigma-Aldrich) and MOPS buffer (20 mM, pH 7.4) in the ratio 1:1 was stirred overnight at room temperature (500 rpm) to saturate both liquids with each other. Afterward, the aqueous and organic layers were separated.

10 mM stock solutions of the test compounds in DMSO (MERCK-Schuchardt, Hohenbrunn, Germany) were prepared by dissolving an exactly weighted amount of the test compound and adding the calculated amount of DMSO. Depending on the lipophilicity, either the 10 mM stock solution was used directly or the stock solution was diluted 1:100 with MOPS buffer to a concentration of 100 μM .

4.6.1.4. General Procedure. In order to determine the $\log D_{7.4}$ value, the micro shake flask method was used.^{43,44} To create physiological conditions, a buffer with pH 7.4 was used to analyze the lipophilicity ($\log D_{7.4}$). The $\log D_{7.4}$ value was determined by using three different volume ratios of buffer and *n*-octanol (1:1, 2:1, and 1:2).

Method LA (standard procedure): The 10 mM DMSO stock solution of the test compound (7.5 μL) was added to three different volumes of MOPS buffer (750, 1000, and 500 μL) in 2 mL Eppendorf tubes. Afterward, the tubes were filled up to 1500 μL with *n*-octanol (750, 500, and 1000 μL). Each ratio was produced as a triplicate. The tubes were vortexed at rt and centrifuged at 4 $^{\circ}\text{C}$ with 16,000 rpm for 2 min.

Method LB (for very hydrophilic compounds): The 100 μM MOPS solution of the test compound (75 μL) was added to three different volumes of MOPS buffer (675, 925, and 425 μL) in 2 mL Eppendorf tubes. *n*-Octanol was added to fill up the tubes to a total volume of 1500 μL (750, 500, and 1000 μL). Each ratio was produced as a triplicate. Afterward, the tubes were vortexed at rt and centrifuged at 4 $^{\circ}\text{C}$ with 16,000 rpm for 2 min.

An aliquot of the aqueous layer was analyzed by LC–MS method LA. For matrix-matched calibration to calculate the $\log D_{7.4}$ value, the samples were diluted with MOPS buffer within a range of 1.56 nM to 1.0 μM or 39 nM to 10 μM . All samples were measured once.

4.6.2. Plasma Protein Binding.^{43,64,65}
4.6.2.1. Instruments and Parameters for LC–MS PPB Analysis. UPLC-UV/MS (Agilent Technologies): degasser: 1260 HiP (G4225A); pump: 1260 Bin Pump (G1212B); autosampler: 1260 HiP ALS (G1367E); column oven: 1290 TCC (G1316C), 30 $^{\circ}\text{C}$; UV/vis detector: 1260 VWD (G1314F); and MS detector: 6120 Quadrupole LC/MS (G1978B). MS source: multimode source (G1978B); ESI mode; and SIM mode (m/z given for each compound). Data acquisition and settings were performed with an OpenLab CDS (ChemStation Edition, Agilent). Guard column: Chiralpak HSA HPLC guard column (2.0 \times 10 mm, 5.0 μm particle size). Main column: Chiralpak HSA HPLC column (Daicel, Eschborn, Germany) (2.0 \times 50 mm, 5.0 μm particle size). Spray chamber: vaporizer temperature: 200 $^{\circ}\text{C}$; drying gas: 12 L/min; nebulizer pressure: 40 psi; capillary voltage: 3000 V; corona current: 4 μA ; charging voltage: 2000 V; fragmentor voltage: 100 V; and drying

gas temperature: 250 °C. 2 mL safe lock tubes (Eppendorf) and 2 mL LC–MS vials (Agilent).

4.6.2.2. LC–MS PPB Method. Eluents: solvent A: NH₄OAc buffer (50 mM, pH 7.4); solvent B: isopropanol; and isocratic elution (A %): 96%. Flow rate: 0.3 mL/min. Stop time: 3.0 min (*D*-glucose, metronidazole, paracetamol, ramipril, salbutamol, and sulfamethoxazole), 8.0 min (propranolol), 10 min (phenytoin), 15 min (haloperidol and imipramine), and 60 min (chlorpromazine and test compounds). Injection volume: 1.0–100 μL (given for each compound, 1.0 μL if not stated otherwise).

4.6.2.3. Chemicals, Solvents, and Stock Solutions. The pH value of an aqueous solution of NH₄OAc (50 mM, Acros Organics, Schwerte, Germany) was adjusted to pH 7.4 with NH₃. 2.0 mM solutions of the reference and the test compounds were prepared from the 10 mM DMSO stock solutions by diluting 1:5 with DMSO (MERCK-Schuchardt, Hohenbrunn, Germany). The final concentration of 20 μM was prepared by further dilution 1:100 with eluent NH₄OAc (50 mM, pH 7.4):isopropanol = 96:4.

4.6.2.4. Method PA (General Procedure). In order to determine the PPB, HPLC was performed. The dead time was determined with *D*-glucose. The following compounds with known PPB were used as reference compounds: metronidazole, paracetamol, salbutamol, sulfamethoxazole, ramipril, propranolol, phenytoin, haloperidol, imipramine, and chlorpromazine. The retention times of these compounds and the test compound were measured three times by the LC–MS PPB method in the SIM mode.

4.6.3. Metabolic Stability In Vitro.^{43,66} **4.6.3.1. Preparation of Liver Microsomes.** Frozen livers (–80 °C) from male C57BL/6 mice were received from Prof. Dr. Martina Düfer from the Institute of Pharmaceutical and Medicinal Chemistry (WWU Münster).

At first, the frozen livers were warmed up at 37 °C for a few minutes and washed with 1.15% (*m/v*) KCl solution at 4 °C. After cutting the livers into small pieces, the livers were homogenized in an Elvehjem–Potter (10 strokes, 3 s, 800 rpm) with cold phosphate buffer (pH 7.4, 0.1 M, 1.0 mL PBS/g liver) containing sodium EDTA (0.5 mM). PBS (pH 7.4, 0.1 M, 3.0 mL PBS/g liver), cooled on ice, was added, and the resulting suspension was centrifuged at 9000g for 20 min at 4 °C. The supernatant was centrifuged again at 40,000g for 90 min at 4 °C. The obtained microsomes pellet was dissolved in PBS (pH 7.4, 0.1 M). Aliquots of 1.0 mL were filled in safe lock Eppendorf tubes and stored at –80 °C.

4.6.3.2. Instruments and Parameters for LC–MS Standard Analysis. UPLC–UV/MS (Agilent Technologies): degasser: 1260 HiP (G4225A); pump: 1260 Bin Pump (G1212B); autosampler: 1260 HiP ALS (G1367E); column oven: 1290 TCC (G1316C), 30 °C; UV/vis detector: 1260 VWD (G1314F); and MS detector: 6120 Quadrupole LC/MS (G1978B). MS source: multimode source (G1978B); ESI mode; and SIM mode (*m/z* given for each compound). Data acquisition and settings were performed with an OpenLab CDS (ChemStation Edition, Agilent). Guard column: Zorbax Eclipse Plus–C18 (Agilent, Waldbronn, Germany) (2.1 mm × 12.5 mm, 5.0 μm particle size). Main column: Zorbax SB–C18 (Agilent, Waldbronn, Germany) (2.1 mm × 50 mm, 1.8 μm particle size). Spray chamber: vaporizer temperature: 200 °C; drying gas: 12 L/min; nebulizer pressure: 40 psi; capillary voltage: 3000 V; corona current: 4 μA; charging voltage: 2000 V; fragmentor voltage: 100 V; and drying gas temperature: 250 °C. 2 mL safe lock tubes (Eppendorf) and 2 mL LC–MS vials (Agilent).

4.6.3.3. LC–MS Standard Method. Eluents: solvent A: H₂O/CH₃CN 95:5 + 0.1% formic acid; solvent B: H₂O/CH₃CN 5:95 + 0.1% formic acid; and gradient elution (A %): 0–2.5 min: gradient from 100 to 0%, 2.5–3.5 min: 0%, 3.5–4.0 min: gradient from 0 to 100%, and 4.0–8.0 min: 100%. Change valve position: after 1.0 min, the valve was switched from “waste” to “MS source”. Flow rate: 0.4 mL/min. Injection volume: 1.0–100 μL (given for each compound, 1.0 μL if not stated otherwise).

4.6.3.4. Chemicals, Solvents, and Stock Solutions. NADPH Na₄ (Carl Roth, Karlsruhe, Germany) was dissolved in phosphate buffer (PBS, 0.1 M, pH 7.4, Sigma–Aldrich, Darmstadt, Germany) to prepare a 2.0 mg/mL solution. MgCl₂ (Honeywell Specialty Chemicals,

Seelze, Germany) was dissolved in bidist. H₂O to a obtain a 0.05 M solution. 1.0 mM solutions of the test compounds were prepared from the 10 mM DMSO stock solutions by diluting 1:10 with DMSO (MERCK–Schuchardt, Hohenbrunn, Germany).

4.6.3.5. Phase I Metabolism (Method MA). NADPHNa₄ (2.0 mg/mL in 0.1 M PBS, 50 μL), MgCl₂ (0.05 M in H₂O, 50 μL), and phosphate buffer (PBS, 0.1 M, 76.8 μL) were mixed in an Eppendorf tube. The test compound (1.0 mM in DMSO, 1.2 μL) and mouse liver microsomes (MLM, 22 μL) were added. Instead of the test compound, imipramine (1.0 mM in DMSO, 1.2 μL) was incubated with mouse liver microsomes as a positive control. The metabolic stability of imipramine using this procedure is well known (20% of parent compound after 90 min incubation). The prepared samples were incubated at 37 °C for 90 min at 900 rpm at the thermomixer (Eppendorf). The incubation was stopped by the addition of CH₃CN/CH₃OH 1:1 (400 μL) to the samples and ice-cooled for 10 min to precipitate the proteins. The samples were centrifuged at 4 °C for 15 min at 16,000 rpm. An aliquot of the supernatant was measured by the LC–MS standard method. An “empty sample” (without test compound, PBS was added to replace the missing volume) was prepared in the same way. Additionally, “blanks” (without NADPH Na₄, PBS was added to replace the missing volume) were prepared according to the same procedure. The test compound (10 mM in DMSO, 1.2 μL) was added after precipitating the proteins under ice-cooling for 10 min.

4.7. Capsaicin Assay, Antiallodynic Activity. In vivo efficacy studies in mice were conducted at the University of Granada, Granada, Spain. Animal care was provided in accordance with institutional (Research Ethics Committee of the University of Granada, Granada, Spain), regional (Junta de Andalucía, Spain), and international (European Communities Council Directive 2010/63) standards. The protocol of the experiments was approved by the Research Ethics Committee of the University of Granada (License number 16/07/2020/083).

Female CD-1 mice (Charles River, Barcelona, Spain) weighing 25–30 g were used for all experiments. The animals were housed in a temperature-controlled room (21 ± 1 °C) with air exchange every 20 min and an automatic 12 h light/dark cycle (8 to 20 h). They were fed a standard laboratory diet and tap water ad libitum until the beginning of the experiments. The experiments were performed during the light phase (9–15 h).

To evaluate the effect of drugs on mechanical allodynia induced by capsaicin, a previously described experimental procedure was used.¹⁸ The compound under study, the prototypical σ₁ antagonist S1RA, or the solvent (5% DMSO) was administered subcutaneously (*s.c.*) to mice 30 min before the intraplantar (*i.pl.*) administration of 20 μL of capsaicin (1 μg in 1% DMSO). 15 min after the *i.pl.* administration of capsaicin, a mechanical punctate stimulation (0.5 g force) was applied with an electronic von Frey device (Dynamic Plantar Aesthesiometer, Ugo Basile, Comerio, Italy) at least 5 mm from the site of injection toward the toes (area of secondary mechanical hypersensitivity), and the paw withdrawal latency time was automatically recorded. Each mouse was tested in three trials at 30 s intervals, and the mean of the three measurements was calculated. A cutoff time of 50 s was used in each trial.

The degree of effect on capsaicin-induced mechanical allodynia was calculated as % antiallodynic effect = [(LTD–LTS)/(CT–LTS)] × 100, where LTD is the latency time for paw withdrawal in drug-treated animals, LTS is the latency time in solvent-treated animals (mean value 13.51 s), and CT is the cutoff time (50 s). The statistical significance of differences between values obtained in the different experimental groups were analyzed with one-way ANOVA, followed by the Bonferroni test. The differences between means were considered statistically significant when the value of *P* was below 0.05.

■ ASSOCIATED CONTENT

Supporting Information

The Supporting Information is available free of charge at <https://pubs.acs.org/doi/10.1021/acs.jmedchem.2c02081>.

Purity data of all the prepared compounds; ^1H , ^{13}C , and NOESY NMR spectra of the prepared compounds; and HPLC chromatograms of the key compounds (PDF)
Molecular formula strings of the prepared compounds (CSV)

AUTHOR INFORMATION

Corresponding Author

Bernhard Wunsch – Institut für Pharmazeutische und Medizinische Chemie, Westfälische Wilhelms-Universität Münster, D-48149 Münster, Germany; orcid.org/0000-0002-9030-8417; Phone: +49-251-8333311; Email: wunsch@uni-muenster.de; Fax: +49-251-8332144

Authors

Luca Blicher – Institut für Pharmazeutische und Medizinische Chemie, Westfälische Wilhelms-Universität Münster, D-48149 Münster, Germany

Rafael González-Cano – Department of Pharmacology, Faculty of Medicine and Biomedical Research Center (Neurosciences Institute), Biosanitary Research Institute ibs. GRANADA, University of Granada, Granada 18016, Spain

Erik Laurini – Molecular Biology and Nanotechnology Laboratory (MolBNL@UniTS), DEA, University of Trieste, 34127 Trieste, Italy; orcid.org/0000-0001-6092-6532

Francisco R. Nieto – Department of Pharmacology, Faculty of Medicine and Biomedical Research Center (Neurosciences Institute), Biosanitary Research Institute ibs. GRANADA, University of Granada, Granada 18016, Spain; orcid.org/0000-0001-9555-0651

Judith Schmidt – Institut für Pharmazeutische und Medizinische Chemie, Westfälische Wilhelms-Universität Münster, D-48149 Münster, Germany

Dirk Schepmann – Institut für Pharmazeutische und Medizinische Chemie, Westfälische Wilhelms-Universität Münster, D-48149 Münster, Germany

Sabrina Priel – Molecular Biology and Nanotechnology Laboratory (MolBNL@UniTS), DEA, University of Trieste, 34127 Trieste, Italy; Department of General Biophysics, Faculty of Biology and Environmental Protection, University of Lodz, 90-136 Lodz, Poland; orcid.org/0000-0001-8380-4474

Complete contact information is available at: <https://pubs.acs.org/10.1021/acs.jmedchem.2c02081>

Notes

The authors declare no competing financial interest.

ACKNOWLEDGMENTS

This work was supported by the INTERREG project “Natural scaffolds/intermediates for drug development”, which is gratefully acknowledged. We thank Jorg Benningshof and Jan Sadownik at Symeres for the separation of diastereomers **8a** and **9a**.

ABBREVIATIONS

Asp, aspartic acid; AV, average; CNS, central nervous system; CT, cutoff time; ΔG_{EXP} , ligand/protein free energy of binding experimentally determined; ΔG_{MD} , ligand/protein free energy of binding determined by MD; DIPEA, diisopropylethylamine; DMP, Dess–Martin periodinane; ED_{50} , median effective dose; Glu, glutamic acid; HPLC, high-performance liquid chroma-

tography; i.p., intraplantar; LLE, lipophilic ligand efficiency; LTD, latency time of drug-treated animals; LTS, latency time of solvent-treated animals; mCPBA, meta-chloroperbenzoic acid; MD, molecular dynamics; MM/PBSA, molecular mechanics/Poisson–Boltzmann surface area; NMDA, N-methyl-D-aspartate; NOE, nuclear Overhauser effect; NOESY, nuclear Overhauser effect spectroscopy; PET, positron emission tomography; PPB, plasma protein binding; PRBFED, per-residue binding free energy deconvolution; SEM, standard error of the mean; s.c., subcutaneously; Tyr, tyrosine

REFERENCES

- (1) Walker, J. M.; Bowen, W. D.; Walker, F. O.; Matsumoto, R. R.; De Costa, B. D.; Rice, K. C. Sigma Receptors: Biology and Function. *Pharmacol. Rev.* **1990**, *42*, 355–402.
- (2) Smith, S. *Sigma Receptors: Their Role in Disease and as Therapeutic Targets*; Springer Berlin Heidelberg: New York, NY, 2016.
- (3) Maurice, T.; Su, T.-P. The Pharmacology of Sigma-1 Receptors. *Pharmacol. Ther.* **2009**, *124*, 195–206.
- (4) van Waarde, A.; Rybczynska, A. A.; Ramakrishnan, N. K.; Ishiwata, K.; Elsinga, P. H.; Dierckx, R. A. J. O. Potential Applications for Sigma Receptor Ligands in Cancer Diagnosis and Therapy. *Biochim. Biophys. Acta, Biomembr.* **2015**, *1848*, 2703–2714.
- (5) Megalizzi, V.; Le Mercier, M.; Decaestecker, C. Sigma Receptors and Their Ligands in Cancer Biology: Overview and New Perspectives for Cancer Therapy. *Med. Res. Rev.* **2012**, *32*, 410–427.
- (6) Xie, F.; Bergmann, R.; Kniess, T.; Deuther-Conrad, W.; Mamat, C.; Neuber, C.; Liu, B.; Steinbach, J.; Brust, P.; Pietzsch, J.; Jia, H. 18F-Labeled 1,4-Dioxo-8-Azaspiro[4.5]Decane Derivative: Synthesis and Biological Evaluation of a σ_1 Receptor Radioligand with Low Lipophilicity as Potent Tumor Imaging Agent. *J. Med. Chem.* **2015**, *58*, 5395–5407.
- (7) Sakata, M.; Kimura, Y.; Naganawa, M.; Oda, K.; Ishii, K.; Chihara, K.; Ishiwata, K. Mapping of Human Cerebral Sigma-1 Receptors Using Positron Emission Tomography and [^{11}C]SA4503. *NeuroImage* **2007**, *35*, 1–8.
- (8) Fischer, S.; Wiese, C.; Große Maestrup, E.; Hiller, A.; Deuther-Conrad, W.; Scheunemann, M.; Schepmann, D.; Steinbach, J.; Wunsch, B.; Brust, P. Molecular Imaging of σ Receptors: Synthesis and Evaluation of the Potent σ_1 Selective Radioligand [^{18}F]-Fluspidine. *Eur. J. Nucl. Med. Mol. Imaging* **2011**, *38*, 540–551.
- (9) Schmidt, H. R.; Zheng, S.; Gurbinar, E.; Koehl, A.; Manglik, A.; Kruse, A. C. Crystal structure of the human σ_1 receptor. *Nature* **2016**, *532*, 527–530.
- (10) Schmidt, H. R.; Betz, R. M.; Dror, R. O.; Kruse, A. C. Structural Basis for Σ_1 Receptor Ligand Recognition. *Nat. Struct. Mol. Biol.* **2018**, *25*, 981–987.
- (11) Rack, E.; Fröhlich, R.; Schepmann, D.; Wunsch, B. Design, synthesis and pharmacological evaluation of spirocyclic σ_1 receptor ligands with exocyclic amino moiety (increased distance 1). *Bioorg. Med. Chem.* **2011**, *19*, 3141–3151.
- (12) Sánchez-Fernández, C.; Montilla-García, Á.; González-Cano, R.; Nieto, F. R.; Romero, L.; Artacho-Cordón, A.; Montes, R.; Fernández-Pastor, B.; Merlos, M.; Baeyens, J. M.; Entrena, J. M.; Cobos, E. J. Modulation of Peripheral μ -Opioid Analgesia by Σ_1 Receptors. *J. Pharmacol. Exp. Ther.* **2014**, *348*, 32–45.
- (13) Chien, C.-C.; Pasternak, G. W. Sigma Antagonists Potentiate Opioid Analgesia in Rats. *Neurosci. Lett.* **1995**, *190*, 137–139.
- (14) Chien, C. C.; Pasternak, G. W. Functional Antagonism of Morphine Analgesia by (+)-Pentazocine: Evidence for an Anti-Opioid σ_1 System. *Eur. J. Pharmacol.* **1993**, *250*, R7–R8.
- (15) Vidal-Torres, A.; de la Puente, B.; Rocasalbas, M.; Touriño, C.; Bura, S. A.; Fernández-Pastor, B.; Romero, L.; Codony, X.; Zamanillo, D.; Buschmann, H.; Merlos, M.; Baeyens, J. M.; Maldonado, R.; Vela, J. M. Sigma-1 Receptor Antagonism as Opioid Adjuvant Strategy: Enhancement of Opioid Antinociception without Increasing Adverse Effects. *Eur. J. Pharmacol.* **2013**, *711*, 63–72.

- (16) Baron, R.; Binder, A.; Wasner, G. Neuropathic pain: diagnosis, pathophysiological mechanisms, and treatment. *Lancet Neurol.* **2010**, *9*, 807–819.
- (17) Cendán, C. M.; Pujalte, J. M.; Portillo-Salido, E.; Montoliu, L.; Baeyens, J. M. Formalin-Induced Pain Is Reduced in Sigma(1) Receptor Knockout Mice. *Eur. J. Pharmacol.* **2005**, *511*, 73–74.
- (18) Entrena, J. M.; Cobos, E. J.; Nieto, F. R.; Cendán, C. M.; Gris, G.; Del Pozo, E.; Zamanillo, D.; Baeyens, J. M. Sigma-1 Receptors Are Essential for Capsaicin-Induced Mechanical Hypersensitivity: Studies with Selective Sigma-1 Ligands and Sigma-1 Knockout Mice. *Pain* **2009**, *143*, 252–261.
- (19) Puente, B. de la; Nadal, X.; Portillo-Salido, E.; Sánchez-Arroyos, R.; Ovalle, S.; Palacios, G.; Muro, A.; Romero, L.; Entrena, J. M.; Baeyens, J. M.; López-García, J. A.; Maldonado, R.; Zamanillo, D.; Vela, J. M. Sigma-1 Receptors Regulate Activity-Induced Spinal Sensitization and Neuropathic Pain after Peripheral Nerve Injury. *Pain* **2009**, *145*, 294–303.
- (20) Nieto, F. R.; Cendán, C. M.; Sánchez-Fernández, C.; Cobos, E. J.; Entrena, J. M.; Tejada, M. A.; Zamanillo, D.; Vela, J. M.; Baeyens, J. M. Role of Sigma-1 Receptors in Paclitaxel-Induced Neuropathic Pain in Mice. *J. Pain* **2012**, *13*, 1107–1121.
- (21) Díaz, J. L.; Cuberes, R.; Berrocal, J.; Contijoch, M.; Christmann, U.; Fernández, A.; Port, A.; Holenz, J.; Buschmann, H.; Laggner, C.; Serafini, M. T.; Burgueño, J.; Zamanillo, D.; Merlos, M.; Vela, J. M.; Almansa, C. Synthesis and Biological Evaluation of the 1-Arylpyrazole Class of σ 1 Receptor Antagonists: Identification of 4-{2-[5-Methyl-1-(Naphthalen-2-Yl)-1 H -Pyrazol-3-Yloxy]Ethyl}-morpholine (S1RA, E-52862). *J. Med. Chem.* **2012**, *55*, 8211–8224.
- (22) Wünsch, B. The σ 1 Receptor Antagonist S1RA Is a Promising Candidate for the Treatment of Neurogenic Pain. *J. Med. Chem.* **2012**, *55*, 8209–8210.
- (23) Bruna, J.; Videla, S.; Argyriou, A. A.; Velasco, R.; Villoria, J.; Santos, C.; Nadal, C.; Cavaletti, G.; Alberti, P.; Briani, C.; Kalofonos, H. P.; Cortinovis, D.; Sust, M.; Vaqué, A.; Klein, T.; Plata-Salamán, C. Efficacy of a Novel Sigma-1 Receptor Antagonist for Oxaliplatin-Induced Neuropathy: A Randomized, Double-Blind, Placebo-Controlled Phase IIa Clinical Trial. *Neurotherapeutics* **2018**, *15*, 178–189.
- (24) Friedrich, D.; Bohlmann, F. Total Synthesis of Various Elemanolides. *Tetrahedron* **1988**, *44*, 1369–1392.
- (25) Hasebein, P.; Frehland, B.; Lehmkuhl, K.; Fröhlich, R.; Schepmann, D.; Wünsch, B. Synthesis and Pharmacological Evaluation of Like- and Unlike-Configured Tetrahydro-2-Benzazepines with the α -Substituted Benzyl Moiety in the 5-Position. *Org. Biomol. Chem.* **2014**, *12*, 5407–5426.
- (26) Miyata, K.; Schepmann, D.; Wünsch, B. Synthesis and σ Receptor Affinity of Regioisomeric Spirocyclic Furopyridines. *Eur. J. Med. Chem.* **2014**, *83*, 709–716.
- (27) Meyer, C.; Neue, B.; Schepmann, D.; Yanagisawa, S.; Yamaguchi, J.; Würthwein, E.-U.; Itami, K.; Wünsch, B. Improvement of σ 1 Receptor Affinity by Late-Stage C–H-Bond Arylation of Spirocyclic Lactones. *Bioorg. Med. Chem.* **2013**, *21*, 1844–1856.
- (28) Schepmann, D.; Frehland, B.; Lehmkuhl, K.; Tewes, B.; Wünsch, B. Development of a Selective Competitive Receptor Binding Assay for the Determination of the Affinity of NR2B Containing NMDA Receptors. *J. Pharm. Biomed. Anal.* **2010**, *53*, 603–608.
- (29) Matsumoto, R. R.; Bowen, W. D.; Tom, M. A.; Vo, V. N.; Truong, D. D.; De Costa, B. R. Characterization of Two Novel σ Receptor Ligands: Antidystonic Effects in Rats Suggest σ Receptor Antagonism. *Eur. J. Pharmacol.* **1995**, *280*, 301–310.
- (30) Hashimoto, K.; London, E. D. Further Characterization of [3H]Ifenprodil Binding to σ Receptors in Rat Brain. *Eur. J. Pharmacol.* **1993**, *236*, 159–163.
- (31) Hashimoto, K.; London, E. D. Interactions of Erythro-Ifenprodil, Threo-Ifenprodil, Erythro-Iodoifenprodil, and Eliprodil with Subtypes of σ Receptors. *Eur. J. Pharmacol.* **1995**, *273*, 307–310.
- (32) Thum, S.; Schepmann, D.; Reinoso, R. F.; Alvarez, I.; Ametamey, S. M.; Wünsch, B. Synthesis and Pharmacological Evaluation of Fluorinated Benzo[7]Annulen-7-Amines as GluN2B-Selective NMDA Receptor Antagonists. *J. Labelled Compd. Radiopharm.* **2019**, *62*, 354–379.
- (33) Schmidt, H. R.; Zheng, S. D.; Gurpinar, E.; Koehl, A.; Manglik, A.; Kruse, A. C. Crystal structure of the human σ 1 receptor. *Nature* **2016**, *532*, 527.
- (34) Kronenberg, E.; Weber, F.; Brune, S.; Schepmann, D.; Almansa, C.; Friedland, K.; Laurini, E.; Pricl, S.; Wünsch, B. Synthesis and Structure-Affinity Relationships of Spirocyclic Benzopyrans with Exocyclic Amino Moiety. *J. Med. Chem.* **2019**, *62*, 4204–4217.
- (35) Kopp, N.; Holtschulte, C.; Börgel, F.; Lehmkuhl, K.; Friedland, K.; Civenni, G.; Laurini, E.; Catapano, C. V.; Pricl, S.; Humpf, H.-U.; Schepmann, D.; Wünsch, B. Novel σ 1 antagonists designed for tumor therapy: structure - activity relationships of aminoethyl substituted cyclohexanes. *Eur. J. Med. Chem.* **2021**, *210*, 112950.
- (36) Holtschulte, C.; Börgel, F.; Westphäliger, S.; Schepmann, D.; Civenni, G.; Laurini, E.; Marson, D.; Catapano, C. V.; Pricl, S.; Wünsch, B. Synthesis of Aminoethyl-Substituted Piperidine Derivatives as σ 1 Receptor Ligands with Antiproliferative Properties. *ChemMedChem* **2022**, *17*, No. e202100735.
- (37) Massova, I.; Kollman, P. A. Combined molecular mechanical and continuum solvent approach (MM-PBSA/GBSA) to predict ligand binding. *Perspect. Drug Discovery Des.* **2000**, *18*, 113–135.
- (38) Alon, A.; Lyu, J.; Braz, J. M.; Tummino, T. A.; Craik, V.; O'Meara, M. J.; Webb, C. M.; Radchenko, D. S.; Moroz, Y. S.; Huang, X.-P.; Liu, Y.; Roth, B. L.; Irwin, J. J.; Basbaum, A. I.; Shoichet, B. K.; Kruse, A. C. Structures of the σ 2 receptor enable docking for bioactive ligand discovery. *Nature* **2021**, *600*, 759–764.
- (39) Gawaskar, S.; Temme, L.; Schreiber, J. A.; Schepmann, D.; Bonifazi, A.; Robaa, D.; Sippl, W.; Strutz-Seeböhm, N.; Seeböhm, G.; Wünsch, B. Design, Synthesis, Pharmacological Evaluation and Docking Studies of GluN2B-Selective NMDA Receptor Antagonists with a Benzo[7]annulen-7-amine Scaffold. *ChemMedChem* **2017**, *12*, 1212–1222.
- (40) Temme, L.; Bechthold, E.; Schreiber, J. A.; Gawaskar, S.; Schepmann, D.; Robaa, D.; Sippl, W.; Seeböhm, G.; Wünsch, B. Negative allosteric modulators of the GluN2B NMDA receptor with phenylethylamine structure embedded in ring-expanded and ring-contracted scaffolds. *Eur. J. Med. Chem.* **2020**, *190*, 112138.
- (41) Leeson, P. D.; Springthorpe, B. The Influence of Drug-like Concepts on Decision-Making in Medicinal Chemistry. *Nat. Rev. Drug Discovery* **2007**, *6*, 881–890.
- (42) Waring, M. J. Lipophilicity in Drug Discovery. *Expert Opin. Drug Discovery* **2010**, *5*, 235–248.
- (43) Börgel, F.; Galla, F.; Lehmkuhl, K.; Schepmann, D.; Ametamey, S. M.; Wünsch, B. Pharmacokinetic Properties of Enantiomerically Pure GluN2B Selective NMDA Receptor Antagonists with 3-Benzazepine Scaffold. *J. Pharm. Biomed. Anal.* **2019**, *172*, 214–222.
- (44) Galla, F.; Bourgeois, C.; Lehmkuhl, K.; Schepmann, D.; Soeberdt, M.; Lotts, T.; Abels, C.; Ständer, S.; Wünsch, B. Effects of Polar κ Receptor Agonists Designed for the Periphery on ATP-Induced Ca^{2+} Release from Keratinocytes. *MedChemComm* **2016**, *7*, 317–326.
- (45) Leach, A. R.; Hann, M. M.; Burrows, J. N.; Griffen, E. J. Fragment Screening: An Introduction. *Mol. Biosyst.* **2006**, *2*, 429.
- (46) Freeman-Cook, K. D.; Hoffman, R. L.; Johnson, T. W. Lipophilic Efficiency: The Most Important Efficiency Metric in Medicinal Chemistry. *Future Med. Chem.* **2013**, *5*, 113–115.
- (47) Entrena, J. M.; Sánchez-Fernández, C.; Nieto, F. R.; González-Cano, R.; Yeste, S.; Cobos, E. J.; Baeyens, J. M. Sigma-1 Receptor Agonism Promotes Mechanical Allodynia After Priming the Nociceptive System with Capsaicin. *Sci. Rep.* **2016**, *6*, 37835.
- (48) Romero, L.; Zamanillo, D.; Nadal, X.; Sánchez-Arroyos, R.; Rivera-Arconada, I.; Dordal, A.; Montero, A.; Muro, A.; Bura, A.; Segalés, C.; Laloya, M.; Hernández, E.; Portillo-Salido, E.; Escriche, M.; Codony, X.; Encina, G.; Burgueño, J.; Merlos, M.; Baeyens, J.; Giraldo, J.; López-García, J. A.; Maldonado, R.; Plata-Salamán, C. R.; Vela, J. M. Pharmacological Properties of S1RA, a New Sigma-1

Receptor Antagonist That Inhibits Neuropathic Pain and Activity-Induced Spinal Sensitization. *Br. J. Pharmacol.* **2012**, *166*, 2289–2306.

(49) de Costa, B. R.; He, X.; Linders, J. T. M.; Dominguez, C.; Gu, Z. Q.; Williams, W.; Bowen, W. Synthesis and Evaluation of Conformationally Restricted N-[2-(3,4-Dichlorophenyl)Ethyl]-N-Methyl-2-(1-Pyrrolidinyl)Ethylamines at σ Receptors. 2. Piperazines, Bicyclic Amines, Bridged Bicyclic Amines, and Miscellaneous Compounds. *J. Med. Chem.* **1993**, *36*, 2311–2320.

(50) Bergkemper, M.; Kronenberg, E.; Thum, S.; Börgel, F.; Daniliuc, C.; Schepmann, D.; Nieto, F. R.; Brust, P.; Reinoso, R. F.; Alvarez, I.; Wünsch, B. Synthesis, Receptor Affinity, and Antiallosteric Activity of Spirocyclic σ Receptor Ligands with Exocyclic Amino Moiety. *J. Med. Chem.* **2018**, *61*, 9666–9690.

(51) Cheallaigh, A. N.; Mansell, D. J.; Toogood, H. S.; Tait, S.; Lygidakis, A.; Scrutton, N. S.; Gardiner, J. M. Chemoenzymatic Synthesis of the Intermediates in the Peppermint Monoterpenoid Biosynthetic Pathway. *J. Nat. Prod.* **2018**, *81*, 1546–1552.

(52) Waddell, T. G.; Ross, P. A. Chemistry of 3,4-Epoxy Alcohols. Fragmentation Reactions. *J. Org. Chem.* **1987**, *52*, 4802–4804.

(53) Ho, T.-L.; Din, Z. U. Practical Synthesis of Menthofuran. *Synth. Commun.* **1989**, *19*, 813–816.

(54) Yung-Chi, C.; Prusoff, W. H. Relationship between the Inhibition Constant (KI) and the Concentration of Inhibitor Which Causes 50 per Cent Inhibition (I50) of an Enzymatic Reaction. *Biochem. Pharmacol.* **1973**, *22*, 3099–3108.

(55) DeHaven-Hudkins, D. L.; Fleissner, L. C.; Ford-Rice, F. Y. Characterization of the binding of [^3H](+)-pentazocine to σ recognition sites in guinea pig brain. *Eur. J. Pharmacol., Mol. Pharmacol.* **1992**, *227*, 371–378.

(56) Mach, R. H.; Smith, C. R.; Childers, S. R. Ibogaine possesses a selective affinity for σ_2 receptors. *Life Sci.* **1995**, *57*, PL57–PL62.

(57) Case, D. A.; Aktulga, H. M.; Belfon, K.; Ben-Shalom, I. Y.; Berryman, J. T.; Brozell, S. R.; Cerutti, D. S.; Cheatham, T. E., III; Cisneros, G. A.; Cruzeiro, V. W. D.; Darden, T. A.; Duke, R. E.; Giambasu, G.; Gilson, M. K.; Gohlke, H.; Goetz, A. W.; Harris, R.; Izadi, S.; Izmailov, S. A.; Kasavajhala, K.; Kaymak, M. C.; King, E.; Kovalenko, A.; Kurtzman, T.; Lee, T. S.; LeGrand, S.; Li, P.; Lin, C.; Liu, J.; Luchko, T.; Luo, R.; Machado, M.; Man, V.; Manathunga, M.; Merz, K. M.; Miao, Y.; Mikhailovskii, O.; Monard, G.; Nguyen, H.; O'Hearn, K. A.; Onufriev, A.; Pan, F.; Pantano, S.; Qi, R.; Rahnamoun, A.; Roe, D. R.; Roitberg, A.; Sagui, C.; Schott-Verdugo, S.; Shajan, A.; Shen, J.; Simmerling, C. L.; Skrynnikov, N. R.; Smith, J.; Swails, J.; Walker, R. C.; Wang, J.; Wang, J.; Wei, H.; Wolf, R. M.; Wu, X.; Xiong, Y.; Xue, Y.; York, D. M.; Zhao, S.; Kollman, P. A. *Amber 2022*; University of California: San Francisco, 2022.

(58) Karakas, E.; Simorowski, N.; Furukawa, H. Subunit arrangement and phenylethanolamine binding in GluN1/GluN2B NMDA receptors. *Nature* **2011**, *475*, 249–253.

(59) Morris, G. M.; Huey, R.; Lindstrom, W.; Sanner, M. F.; Belew, R. K.; Goodsell, D. S.; Olson, A. J. AutoDock4 and AutoDockTools4: Automated docking with selective receptor flexibility. *J. Comput. Chem.* **2009**, *30*, 2785–2791.

(60) Jorgensen, W. L.; Chandrasekhar, J.; Madura, J. D.; Impey, R. W.; Klein, M. L. Comparison of simple potential functions for simulating liquid water. *J. Chem. Phys.* **1983**, *79*, 926–935.

(61) Massova, I.; Kollman, P. A. Combined molecular mechanical and continuum solvent approach (MM-PBSA/GBSA) to predict ligand binding. *Perspect. Drug Discovery Des.* **2000**, *18*, 113–135.

(62) Tsui, V.; Case, D. A. Theory and applications of the generalized Born solvation model in macromolecular simulations. *Biopolymers* **2000**, *56*, 275–291.

(63) Pettersen, E. F.; Goddard, T. D.; Huang, C. C.; Couch, G. S.; Greenblatt, D. M.; Meng, E. C.; Ferrin, T. E. UCSF Chimera?A visualization system for exploratory research and analysis. *J. Comput. Chem.* **2004**, *25*, 1605–1612.

(64) Butsch, V.; Börgel, F.; Galla, F.; Schwegmann, K.; Hermann, S.; Schäfers, M.; Riemann, B.; Wünsch, B.; Wagner, S. Design, (Radio)Synthesis, and in Vitro and in Vivo Evaluation of Highly

Selective and Potent Matrix Metalloproteinase 12 (MMP-12) Inhibitors as Radiotracers for Positron Emission Tomography. *J. Med. Chem.* **2018**, *61*, 4115–4134.

(65) Konken, C. P.; Heßling, K.; Thale, I.; Schelhaas, S.; Dabel, J.; Maskri, S.; Bulk, E.; Budde, T.; Koch, O.; Schwab, A.; Schäfers, M.; Wünsch, B. Imaging of the Calcium Activated Potassium Channel 3.1 (KCa3.1) in Vivo Using a Senicapoc-Derived Positron Emission Tomography Tracer. *Arch. Pharm.* **2022**, *355*, 2200388.

(66) Wiese, C.; Große Mastrup, E.; Galla, F.; Schepmann, D.; Hiller, A.; Fischer, S.; Ludwig, F.-A.; Deuther-Conrad, W.; Donat, C. K.; Brust, P.; Büter, L.; Karst, U.; Wünsch, B. Comparison of in Silico, Electrochemical, in Vitro and in Vivo Metabolism of a Homologous Series of (Radio)Fluorinated σ_1 Receptor Ligands Designed for Positron Emission Tomography. *ChemMedChem* **2016**, *11*, 2445–2458.

Recommended by ACS

Discovery of a Promising Fluorine-18 Positron Emission Tomography Radiotracer for Imaging Sphingosine-1-Phosphate Receptor 1 in the Brain

Lin Qiu, Zhude Tu, *et al.*

MARCH 16, 2023
JOURNAL OF MEDICINAL CHEMISTRY

READ 

Targeting Receptor-Interacting Protein Kinase 1 by Novel Benzothiazole Derivatives: Treatment of Acute Lung Injury through the Necroptosis Pathway

Xinqi Zhang, Chunlin Zhuang, *et al.*

MARCH 12, 2023
JOURNAL OF MEDICINAL CHEMISTRY

READ 

Discovery of a Potent and Selective CCR8 Small Molecular Antagonist IPG7236 for the Treatment of Cancer

Yong Wu, Guo-Huang Fan, *et al.*

MARCH 29, 2023
JOURNAL OF MEDICINAL CHEMISTRY

READ 

Novel Aryl Sulfonamide Derivatives as NLRP3 Inflammasome Inhibitors for the Potential Treatment of Cancer

Valentina Albanese, Carlotta Giorgi, *et al.*

MARCH 27, 2023
JOURNAL OF MEDICINAL CHEMISTRY

READ 

Get More Suggestions >